The RNA-binding protein Mex3b regulates the spatial organization of the Rap1 pathway

Maïlys Le Borgne, Nicolas Chartier, Karine Buchet-Poyau, Olivier Destaing, Eva Faurobert, Chantal Thibert, Jean-Pierre Rouault, Julien Courchet, Didier Nègre, Daniel Bouvard, et al.

© 2014. Published by The Company of Biologists Ltd | Development (2014) 141, 2096-2107 doi:10.1242/dev.108514

RESEARCH ARTICLE

The RNA-binding protein Mex3b regulates the spatial organization of the Rap1 pathway

Maïlys Le Borgne[1], Nicolas Chartier[1], Karine Buchet-Poyau[2], Olivier Destaing[1], Eva Faurobert[1], Chantal Thibert[1], Jean-Pierre Rouault[3], Julien Courchet[4], Didier Nègre[5], Daniel Bouvard[1], Corinne Albiges-Rizo[1], Sophie Rousseaux[1], Saadi Khochbin[1], Dominique Segretain[6,7], Pascale Crépieux[8], Florian Guillou[8], Philippe Durand[3], Marie-Hélène Perrard[3] and Marc Billaud[1,*]

ABSTRACT

The four related mammalian MEX-3 RNA-binding proteins are evolutionarily conserved molecules for which the *in vivo* functions have not yet been fully characterized. Here, we report that male mice deficient for the gene encoding Mex3b are subfertile. Seminiferous tubules of *Mex3b*-deficient mice are obstructed as a consequence of the disrupted phagocytic capacity of somatic Sertoli cells. In addition, both the formation and the integrity of the blood-testis barrier are compromised owing to mislocalization of N-cadherin and connexin 43 at the surface of Sertoli cells. We further establish that Mex3b acts to regulate the cortical level of activated Rap1, a small G protein controlling phagocytosis and cell-cell interaction, through the activation and transport of Rap1GAP. The active form of Rap1 (Rap1-GTP) is abnormally increased at the membrane cortex and chemically restoring Rap1-GTP to physiological levels rescues the phagocytic and adhesion abilities of Sertoli cells. Overall, these findings implicate Mex3b in the spatial organization of the Rap1 pathway that orchestrates Sertoli cell functions.

KEY WORDS: MEX-3, RNA-binding proteins, Rap1, Phagocytosis, Sertoli cell, Mouse

INTRODUCTION

RNA-binding proteins (RBPs) are central effectors in the control of co- and post-transcriptional mechanisms that contribute to a diverse array of cellular events (Hogan et al., 2008). Recent large scale analyses have further revealed the role of RBPs and their cognate target RNAs in the assembly of multimolecular complexes at specific cellular sites and in the morphological organization of cells (de Hoog et al., 2004; Lécuyer et al., 2007). However, although mRNA interactome studies have provided evidence that RBPs constitute a very large family comprising >1100 proteins in human (Baltz et al., 2012; Castello et al., 2012; Ray et al., 2013), their functions in mammals have not been extensively explored *in vivo* yet.

[1]INSERM, U823; Université Joseph Fourier-Grenoble 1; Institut Albert Bonniot, Grenoble F-38700, France. [2]Hospices Civils de Lyon, Pôle Information Médicale Evaluation Recherche, Lyon F-69003, France. [3]Institut de Génomique Fonctionnelle de Lyon, UMR5242 CNRS/INRA/UCBL/ENS, Ecole Normale Supérieure de Lyon, 46, allée d'Italie, Lyon 69364, Cedex 07, France. [4]Columbia University Department of Neurosciences, New York, NY 10032, USA. [5]Université de Lyon, Inserm, EVIR, U758, Human Virology Department, Ecole Normale Supérieure de Lyon, Université Lyon 1, Lyon F-69007, France. [6]UMR S775, University Paris Descartes, 45 rue des Saints Pères, Paris 75006, France. [7]University of Versailles, Saint Quentin 78035, France. [8]Physiologie de la Reproduction et des Comportements, UMR 7247 INRA-CNRS-Université de Tours, Nouzilly 37380, France.

*Author for correspondence (Marc.Billaud@ujf-grenoble.fr)

Received 29 January 2014; Accepted 14 March 2014

We and others have characterized a novel family of four mammalian RBPs, called MEX3A to MEX3D (Buchet-Poyau et al., 2007; Donnini et al., 2004). The *MEX-3* gene, initially discovered in *Caenorhabditis elegans* (Draper et al., 1996; Hunter and Kenyon, 1996), was found to encode an RBP acting as a translation repressor that specifies the fate of posterior blastomeres during early embryogenesis (Hunter and Kenyon, 1996). Furthermore, MEX-3 together with the RNA-binding protein GLD-1 is essential in maintaining the germline totipotency in the nematode (Ciosk et al., 2006). MEX-3 proteins contain two tandem KH (hnRNP K homology) domains that bind RNA, and mammalian MEX-3 orthologs possess a RING finger motif located at the carboxy-terminal end (Buchet-Poyau et al., 2007). A consensus RNA sequence bound by the *C. elegans* MEX-3, consisting of a bipartite recognition element named MRE, has been defined and mapped in the 3′UTR of >25% of the worm genes (Pagano et al., 2009).

Since their initial description, several reports have sustained the idea that mammalian MEX-3 proteins play several roles in the control of RNA metabolism (Pereira et al., 2013a). MEX3A and MEX3B proteins localize in P-bodies and stress granules, two structures involved in the storage and turnover of mRNAs (Buchet-Poyau et al., 2007; Courchet et al., 2008). MEX3A controls the polarity and stemness of intestinal epithelial cells through the downregulation of the mRNA encoding the CDX2 transcription factor (Pereira et al., 2013b) and, in addition, exhibits a transforming activity when overexpressed in gastric epithelial cells (Jiang et al., 2012). Furthermore, MEX3C and an isoform of MEX3D called TINO control, respectively, the stability of the transcripts coding for the HLA-A2 MHC class I molecule and the anti-apoptotic protein BCL2 (Cano et al., 2012; Donnini et al., 2004). Interestingly, MEX3C acts as a suppressor of chromosomal instability (Burrell et al., 2013), but the RNA-dependent mechanisms involved in this process remain to be determined. Finally, mice with a gene trap insertion in the *Mex3c* locus display postnatal growth retardation, a skeletal phenotype linked to the impaired translation of the mRNA encoding the insulin-like growth factor 1 in bone-forming cells (Jiao et al., 2012a). This *Mex3c* mutation has also been found to enhance mouse energy expenditure, probably through the action of Mex3c in a subpopulation of hypothalamic neurons controlling energy metabolism (Jiao et al., 2012b).

To gain further insight into the function of mammalian MEX-3 homologs, we disrupted the *Mex3b* gene in mouse. We now report that null mice are subfertile owing to a dysfunction of somatic cells in the gonads. In males, the lack of Mex3b impaired the phagocytic properties of Sertoli cells and led to a disorganization of the junctional complexes created between adjacent Sertoli cells that form the blood-testis barrier (BTB). Investigation of the underlying mechanism revealed an unexpected function of Mex3b in the

Development (2014) 141, 2096-2107 doi:10.1242/dev.108514

regulation of the spatial activation of Rap1 (Rap1a – Mouse Genome Informatics), a small GTPase protein implicated in the control of phagocytosis and cell adhesion, through the stimulation and the recruitment of the Rap1 GTPase-activating protein (Rap1GAP) at the inner face of the plasma membrane.

RESULTS

Histological structure of the gonads is disorganized in *Mex3b* null mice

To explore Mex3b functions *in vivo*, we generated mice carrying a conditional *Mex3b* allele with two *loxP* DNA sequences framing exon 2, which encodes 463 amino acids out of the 576 amino acids of the Mex3b protein (Fig. 1A). Heterozygous mice carrying one copy of the null allele were generated through crosses with *Nestin-Cre* transgenic strains that led to the excision of the floxed allele during gametogenesis (Betz et al., 1996). The intercross of $Mex3b^{+/-}$ mice and the genotyping of the resulting offspring confirmed the generation of *Mex3b* null mice (Fig. 1B). Subsequent molecular analyses showed the absence of the *Mex3b* mRNA (supplementary material Fig. S1A) and protein in both mouse embryonic fibroblasts (MEFs) and testis extracts prepared from $Mex3b^{-/-}$ animals (Fig. 1C; supplementary material Fig. S1B). *Mex3b* null mice were born at expected Mendelian ratio, but 30% of these mice died on the first day after birth (supplementary material Fig. S1C). However, no gross abnormalities were observed upon macroscopic examination. The animals surviving to adulthood were smaller and displayed reduced body weight, a statural and weight deficit that was maintained throughout their lives. Upon breeding of the $Mex3b^{+/-}$ heterozygous mice, we observed that the number of pups per month and per female was significantly reduced (0.66 for the breeding of male and female $Mex3b^{+/-}$ mice compared with 0.8 for the breeding of wild-type mice) (Table 1). This decrease was even more pronounced when null male or females were crossed to the wild-type mice (0.39 and 0.35, respectively) or when $Mex3b^{-/-}$ animals were intercrossed (0.33). This effect could not be ascribed to a sexual behavior phenotype of $Mex3b^{+/-}$ or $Mex3b^{-/-}$ animals, because vaginal plugs were daily observed in females after pairing.

Because MEX-3 contributes to the maintenance of the *C. elegans* germline, we decided to investigate further the effects of its deletion on the histology of mouse gonads. Examination of secondary follicle in ovaries of 6-month-old $Mex3b^{-/-}$ female mice revealed a gross disorganization of the granulosa layers with apparent cellular piknosis (supplementary material Fig. S1D). In $Mex3b^{-/-}$ males, the analysis of testes cross-sections of animals ranging from 3 to 6 months of age showed that the architecture of the seminiferous epithelium was altered significantly (Fig. 1E). At 6 months, the lumen within a third of the seminiferous tubules was obstructed (Fig. 1E), a phenotype that did not worsen with aging up to 18 months. We predicted that this obstructive phenotype would decrease the effective sperm count in *Mex3b* null males. Indeed, when we quantified the number of sperm cells flushed from the caudal epididymis of $Mex3b^{-/-}$ males versus wild-type males, we found a two- to threefold reduction in the sperm count compared with that of the wild type at 40 days and at 3 months (Fig. 1D). However, under microscopic observation we observed neither overt abnormalities of spermatozoan morphology, nor sperm cell motility

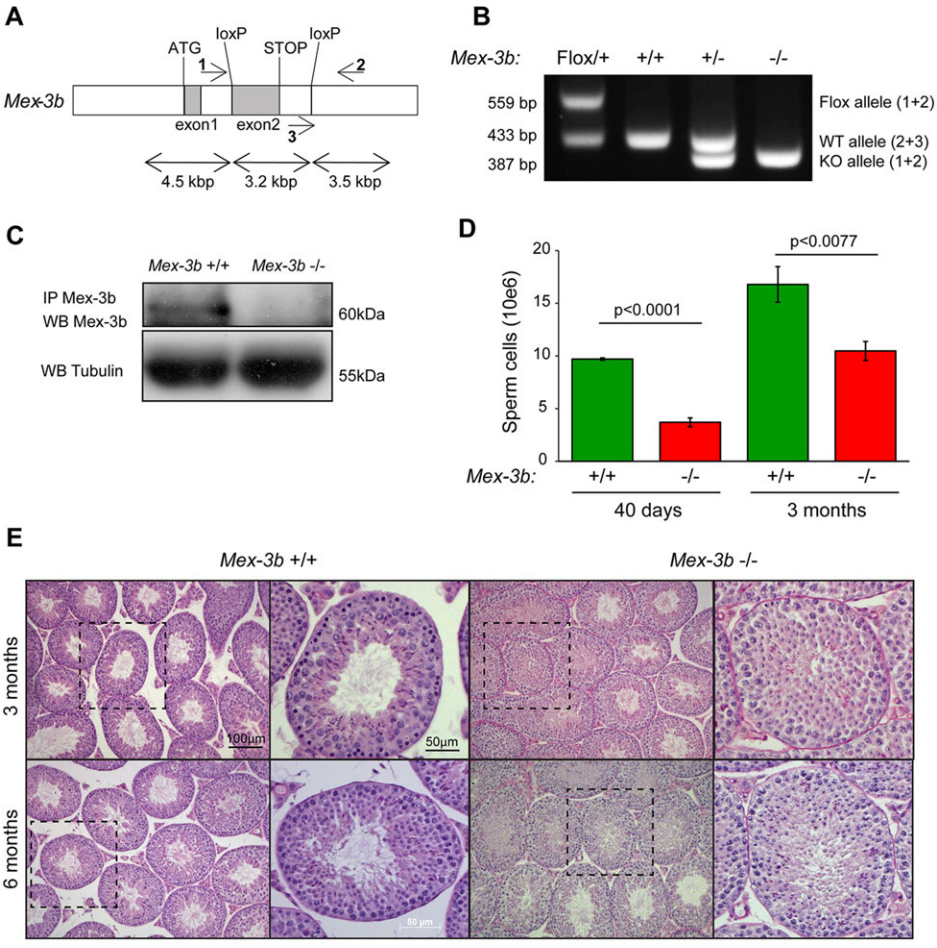

Fig. 1. Genetic ablation of *Mex3b* causes fertility defects in mice. (A) Schematic of the wild-type *Mex3b* allele flanked by *LoxP* sequences. (B) Genotyping of heterozygous *Mex3b* floxed mice (*Mex3b*$Flox^{/+}$), wild-type ($Mex3b^{+/+}$), heterozygous ($Mex3b^{+/-}$) and nullizygous ($Mex3b^{-/-}$) mice. Positions of the different alleles are indicated. (C) Western blot analysis of endogenous Mex3b immunoprecipitated from mouse embryonic fibroblasts (MEFs) with the indicated *Mex3b* genotypes. (D) Number of sperm cells isolated from the epididymis of wild-type and *Mex3*b-deficient mice at different ages (n=5 mice per group; error bars indicate s.e.m.). (E) Periodic Acid Schiff staining of testes sections from mice with the indicated *Mex3b* genotypes. Areas within dashed boxes are shown at higher magnification on the right, showing representative stage seminiferous tubes. The tubular lumen were empty in control mice (stages IV and XI), whereas those of $Mex3b^{-/-}$ mice were obstructed even in early stages of the seminiferous epithelium (stages I-II and VI).

Development (2014) 141, 2096-2107 doi:10.1242/dev.108514

Table 1. Fertility assessment of *Mex3b* knockout mice

Crosses	Fertility*
Male +/+ × female +/+ (*n*=5)	0.8
Male +/– × female +/– (*n*=9)	0.66
Male –/– × female +/+ (*n*=6)	0.39
Male +/+ × female –/– (*n*=6)	0.35
Male –/– × female –/– (*n*=6)	0.33

*The average number of pups per female per month during the period of fertility.

defects. We confirmed that *Mex3b* is expressed in Sertoli cells as well as in pachytene spermatocyte and round spermatids; although the level of *Mex3b* mRNA was very low in pachytene spermatocytes (supplementary material Fig. S1E). The three other Mex3 genes are also expressed in total testis and have a pattern of expression similar to that of *Mex3b* (supplementary material Fig. S1E). Importantly, we did not observe any compensatory increase in the expression of the three other mex-3 homologs in $Mex3b^{-/-}$ testes and in $Mex3b^{-/-}$ Sertoli cells (supplementary material Fig. S1F). Thus, these data indicate that the knockout of *Mex3b* adversely affects the histological architecture of the gonads in females and males and further suggest that the lack of *Mex3b* perturbs the functions of gonadal somatic cells, i.e. granulosa and Sertoli cells, resulting in the observed subfertility.

The loss of *Mex3b* specifically affects Sertoli cells

Taking these findings into consideration, we chose to focus our study on the role of Mex3b in spermatogenesis. The seminiferous epithelium is composed of two cell types: the germ and Sertoli cells. Somatic Sertoli cells are large polarized cells that extend from the basement membrane to the lumen of the tubules. These cells act as a stem cell niche and a nurturing microenvironment for the germ cells during their differentiation from diploid spermatogonia to haploid spermatozoa (Russell and Peterson, 1985). About 30 germ cells at different stages of their maturation interact with each Sertoli cell. Specific types of junctions between adjacent Sertoli cells form the BTB, which constitutes an immune-privileged site protecting postmeiotic germ cells (Cheng and Mruk, 2012). Finally, Sertoli cells clear apoptotic germ cells and residual bodies that are derived from the excess cytoplasmic content and organelles shed by spermatids during their differentiation.

To investigate whether the phenotype observed in the seminiferous tubules resulted from a perturbation of the Sertoli or of the germ cell functions, cross-section of tubules were immunostained with an anti-vimentin antibody. In the testis, vimentin is specifically expressed in Sertoli cells, allowing us to quantify the number of Sertoli cells, pachytene spermatocytes and round spermatids (see Materials and Methods) (Fig. 2A). In male mice aged from 1 to 18 months, we reproducibly observed a significant increase of the number of Sertoli cells in the $Mex3b^{-/-}$ seminiferous tubules compared with the wild type (supplementary material Fig. S2A). However, the ratio between germ and Sertoli cells was significantly decreased in the $Mex3b^{-/-}$ testes (Fig. 2B), indicating that the increase of the number of Sertoli cells was not accompanied by a similar augmentation of the number of germ cells. This effect may reflect a decrease of tubule diameters in the $Mex3b^{-/-}$ testes and a clustering of Sertoli cells secondary to a reduction in the number of germ cells. However, measurement of the average diameter of the tubules in $Mex3b^{+/+}$ and $Mex3b^{-/-}$ testes did not show a significant difference, ruling out this explanation (supplementary material Fig. S2B). Altogether, the observed phenotype was compatible with a Sertoli cell defect leading to an unbalanced ratio between the number of Sertoli and germ cells.

We then investigated whether the disruption of Mex3b impacted on the differentiation of Sertoli cells. For that purpose, we determined by quantitative RT-PCR the level of the mRNA coding for clusterin, the major protein synthesized by differentiated Sertoli cells that is deposited on sperm membranes (Plotton et al., 2005). As shown in Fig. 2C, there was no significant difference of the clusterin/vimentin mRNA ratio between wild-type and $Mex3b^{-/-}$ Sertoli cells. We also quantified transferrin, inhibin and lactate dehydrogenase A (*Ldha*) mRNA. Transferrin is an iron transporter implicated in the regulation of residual bodies phagocytosis by Sertoli cells (Yefimova et al., 2008); inhibin B is produced in the testis, mainly by Sertoli cells and its expression positively correlates with Sertoli cell function and spermatogenesis (O'Connor and de Kretser, 2004); finally, lactate dehydrogenase A (LDHA) is expressed by differentiated Sertoli cells and the lactate produced from pyruvate by LDHA is exported and used by germ cells as an energy metabolite (Boussouar and Benahmed, 2004). As indicated in Fig. 2C, we observed solely a weak but significant increase of *Ldha* transcript in the $Mex3b^{-/-}$ Sertoli cells. Taken together, these data indicate that the lack of *Mex3b* results in a significant increase in the number of Sertoli cells, and alters the germ cell/Sertoli cell ratio, but without affecting the apparent differentiation of Sertoli cells.

To ascertain that the testis phenotype was due to an intrinsic defect specific to Sertoli cells, we generated mice with a disruption of *Mex3b* targeted to this cell type. For that purpose, we crossed $Mex3b^{Flox/Flox}$ mice with transgenic mice expressing the Cre recombinase under the transcriptional control of the anti-Müllerian hormone (Amh) gene promoter (Lécureuil et al., 2002). In male testis, AMH is uniquely expressed in Sertoli cells and not in germ cells. Previous studies using this *AMH::Cre* transgenic strain have shown that the Cre activity is detectable in Sertoli cells from mouse embryonic day 15 to adulthood (Lécureuil et al., 2002). Breeding of *Mex3b* floxed males expressing the Cre recombinase under the control of the *Amh* promoter with *Mex3b* floxed females leads to the same reduction of fertility than that observed upon breeding of *Mex3b* null male mice with wild-type females (Table 2). These data indicate that the targeted invalidation of *Mex3b* to Sertoli cells recapitulates the male subfertility phenotype observed with the total *Mex3b* knockout.

Consistently, histological examination of cross-sections of testis of 1- and 2-month-old offspring revealed obstructed seminiferous tubules at a ratio that was highly similar to that observed in *Mex3b* null mice (Fig. 2D). However, we observed neither a perinatal lethality nor an effect on postnatal growth of these mice. We further confirmed that the *Mex3b* mRNA was specifically decreased in the testis and not in other organs (Fig. 2E). Quantification of the number of germ cells and Sertoli cells showed a decrease in their ratio that was in the same order of magnitude as the effect observed in *Mex3b* null mice (Fig. 2F). Thus, these data establish that the testis phenotype caused by the lack of *Mex3b* is largely due to a defect specific to Sertoli cells.

Mex3b function promotes phagocytosis

The clogged lumen of seminiferous tubules observed in the *Mex3b* null mice could result from an aberrant accumulation of residual bodies as a consequence of a disruption of Sertoli cell phagocytic function. Accordingly, residual bodies were present in early stages of the cycle of *Mex3b* null mice and $Mex3b^{Flox/Flox}$*; AMH::Cre* mice seminiferous epithelium (stages II-III, V and VI), indicating the persistence of material released from elongated spermatids at previous stages (stages VIII-XI) that were not eliminated by Sertoli cells. To test the hypothesis of a Sertoli cell phagocytic dysfunction in the absence of *Mex3b*, we immunolabeled 15-lipoxygenase (15-LOX;

Development (2014) 141, 2096-2107 doi:10.1242/dev.108514

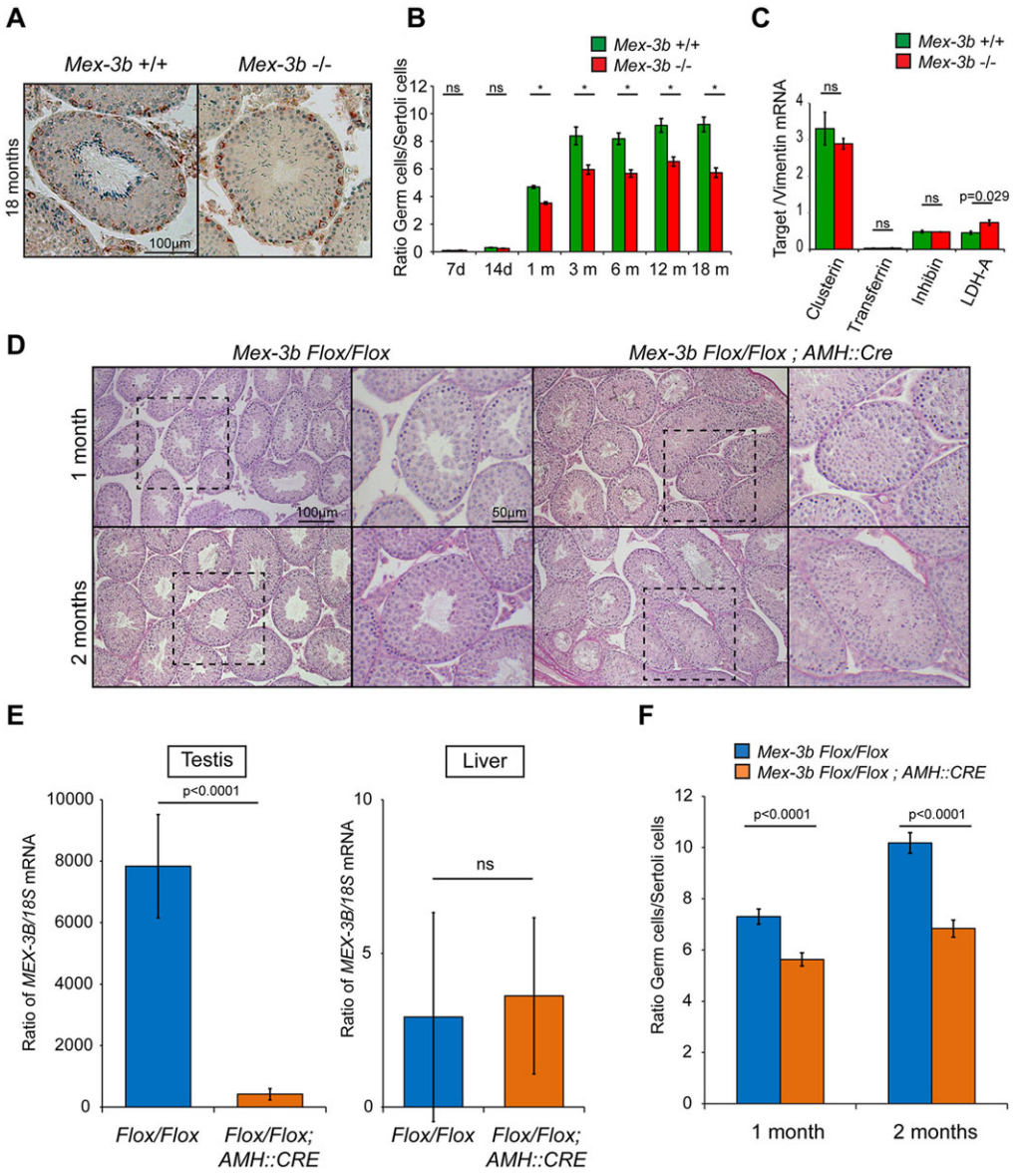

Fig. 2. Mex3b function is specifically required in Sertoli cells. (A) Vimentin immunostaining on cross-sections from 18-month-old mouse testes with the indicated *Mex3b* genotypes. (B) Ratio between germ cells (pachytene spermatocytes or round spermatids) and Sertoli cells in seminiferous tubules from wild-type and *Mex3b*-deficient mice at different ages (d, days; m, months). Sertoli cells were identified as vimentin-positive cells and germ cells as vimentin-negative cells (n=6 mice/group, 30 seminiferous tubules/mouse). *P<0.01. (C) Expression of genes implicated in Sertoli cell differentiation (target genes) quantified by RT-qPCR using mRNA purified from whole testis of 1-month-old mice. The ratio between target and vimentin mRNAs was used to normalize the total number of Sertoli cells per testis. (D) Periodic Acid Schiff staining of testicular cross-sections from floxed (*Mex3b*$^{Flox/Flox}$) and Sertoli-specific deficient mice aged 1 and 2 months. Areas within dashed boxes are shown at higher magnification on the right. Tubule lumens of *Mex3b*$^{Flox/Flox}$ mice were empty (stages VIII and XI) whereas those of *Mex3b*$^{Flox/Flox}$*; AMH::Cre* were obstructed at stages V and VIII. (E) RT-qPCR analysis of *Mex3b* transcripts using testis and liver extracts of 1-month-old mice. The invalidation of *Mex3b* in Sertoli cells was determined by quantifying *Mex3b* mRNA levels normalized to the ribosomal *18S* mRNA levels in whole testes extracts. Quantification of *Mex3b* transcript in the liver was used as a control. One representative experiment out of three independent experiments is shown. (F) Ratio between germ and Sertoli cells in seminiferous tubules from floxed and Sertoli-specific deficient mice aged 1 and 2 months (n=6 mice/group, 30 seminiferous tubules/mouse). Error bars represent s.e.m. n.s., not significant.

also known as Alox15), an enzyme that peroxidizes lipids and is known to concentrate within residual bodies (Fischer et al., 2005). As depicted in Fig. 3A, obstructed tubules present in the *Mex3b*$^{-/-}$ testes showed a marked staining with the anti-15-LOX antibody compared with the tubules of wild-type animals. The same increase of 15-LOX labeling was observed in the tubules of mice with a disruption of the *Mex3b* locus targeted to Sertoli cells (supplementary material Fig. S3A). Furthermore, Hematoxylin and Scarlett Eosin stained pink the tissue obstructing the tubules, thus confirming that this material was of cytoplasmic origin (supplementary material Fig. S3B). Thus, we conclude that residual bodies accumulate abnormally in the lumen of the tubules of *Mex3b* knockout mice.

To investigate whether this phenotype resulted from a phagocytic defect, primary culture of Sertoli cells established from *Mex3b*$^{-/-}$ and wild-type mice were incubated with fluorescent latex beads and their phagocytic capacity was assessed. As shown in Fig. 3B, *Mex3b*-deficient Sertoli cells showed a reduced ability to engulf beads compared with the wild-type Sertoli cells. This phagocytic impairment was not due to a recognition defect of the latex particle as we observed the same capacity of wild-type and *Mex3b*$^{-/-}$ Sertoli cells to absorb

Development (2014) 141, 2096-2107 doi:10.1242/dev.108514

Table 2. Fertility assessment of Sertoli-specific *Mex3b*-deficient mice

Crosses	Fertility*
Male *Flox/Flox* × female *Flox/Flox* (*n*=6)	0.76
Male *AMH:Cre; Flox/Flox* × female *Flox/Flox* (*n*=6)	0.37
Male *AMH:Cre; Flox/Flox* × female *AMH:Cre; Flox/Flox* (*n*=6)	0.31

*The average number of pups per female per month during the period of fertility.

beads when placed at 4°C. To confirm these results, Mex3b was knocked down in the TM4 cell line derived from non-transformed BALB/C mouse Sertoli cells (Mather, 1980). With this RNAi approach, we were able to block Mex3b expression specifically (supplementary material Fig. S4A) without affecting the expression of other Mex3 proteins (supplementary material Fig. S4B). Furthermore, using lentiviruses expressing human *MEX3B* mRNA, which was insensitive to siRNA targeting mouse *Mex3b* mRNA, we performed rescue experiments by using the human MEX3B wild-type protein fused to the green fluorescent protein (GFP) (supplementary material Fig. S4C). Similar to what we observed in primary Sertoli cells, the reduction of *Mex3b* levels in TM4 drastically decreased their capacity to ingest latex beads (Fig. 3C). In addition, phagocytosis was restored upon re-expression of the wild-type MEX3B (Fig. 3C). Finally, we studied the expression of the Scl11a2 iron transporter (also called Nramp2/DMT1), which is located in the phagosome of Sertoli cells (Jabado et al., 2002), and of the class B scavenger receptor type I (SR-BI; Scarb1 – Mouse Genome Informatics), which contributes to the phagocytic process of this cell type (Nakagawa et al., 2004). However, qRT-PCR analysis did not reveal significant variation of the mRNA encoding these two proteins when TM4 cells transfected with scramble siRNA were compared with TM4 cells knocked down for Mex3b (supplementary material Fig. S3C).

The previous data indicate that Mex3b is a regulator of phagocytosis in Sertoli cells and thus raise the idea that this protein may exhibit a similar function in professional phagocytic cells. To address this question, phagocytosis assays using the same conditions defined for Sertoli cells were applied to the primary cultures of macrophages differentiated from bone marrow mononuclear cells and showed a consistent 50% reduction in the number of beads per *Mex3b*$^{-/-}$ macrophage compared with the wild type (supplementary material Fig. S3D). Collectively, these results demonstrate that Mex3b function is required for phagocytosis in Sertoli cells as well as in macrophages.

Mex3b controls cell-cell adhesion

Sertoli cells form the BTB, allowing a physical separation between blood vessels and the seminiferous tubules through strong intercellular adhesion. Therefore, we next examined the consequences of *Mex3b* ablation on cell-cell interaction between Sertoli cells. For that purpose, we performed an ultrastructural analysis on ultra-thin sections of testes. As depicted in Fig. 4A, Sertoli cells in control testes are well organized and the BTB is lined with endoplasmic reticulum cisternae and clearly delimited. By contrast, the basal region of *Mex3b*$^{-/-}$ Sertoli cells appears distended and locally interrupted, revealing an expansion of

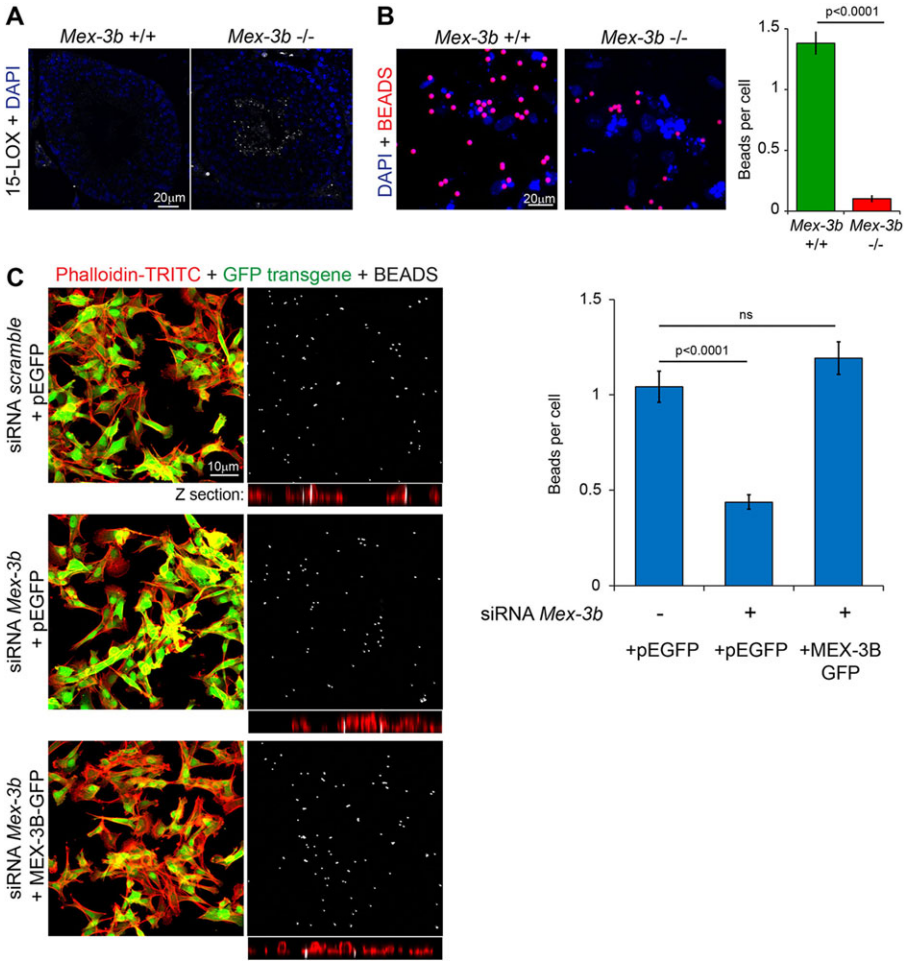

Fig. 3. Phagocytic function of Sertoli cells depends on Mex3b. (A) Immunodetection of the residual bodies component 15-lipoxygenase (white) on cross-sections of 6-month-old mouse testes of the indicated *Mex3b* genotypes. Stage IV seminiferous tubes are shown. Nuclei were stained with DAPI. (B) Epifluorescent images showing latex beads (red) phagocytosed by primary Sertoli cells isolated from wild-type and *Mex3b*$^{-/-}$ mouse testes. Nuclei were stained with DAPI. Histogram indicates the average number of phagocytosed beads per DAPI-stained cell (*n*=200 cells per condition). (C) Projection of confocal sections showing latex beads (white) phagocytosed by TM4 Sertoli cells depleted for endogenous Mex3b by siRNA and re-expressing the human MEX3B protein fused to GFP. Cells were counterstained with phalloidin-TRITC and *z*-sections of confocal acquisition are depicted to show bead incorporation inside the cells. Histogram indicates the average numbers of engulfed fluorescent beads per phalloidin-TRITC-stained cell (*n*=200 cells per condition). Error bars represent s.e.m.

Development (2014) 141, 2096-2107 doi:10.1242/dev.108514

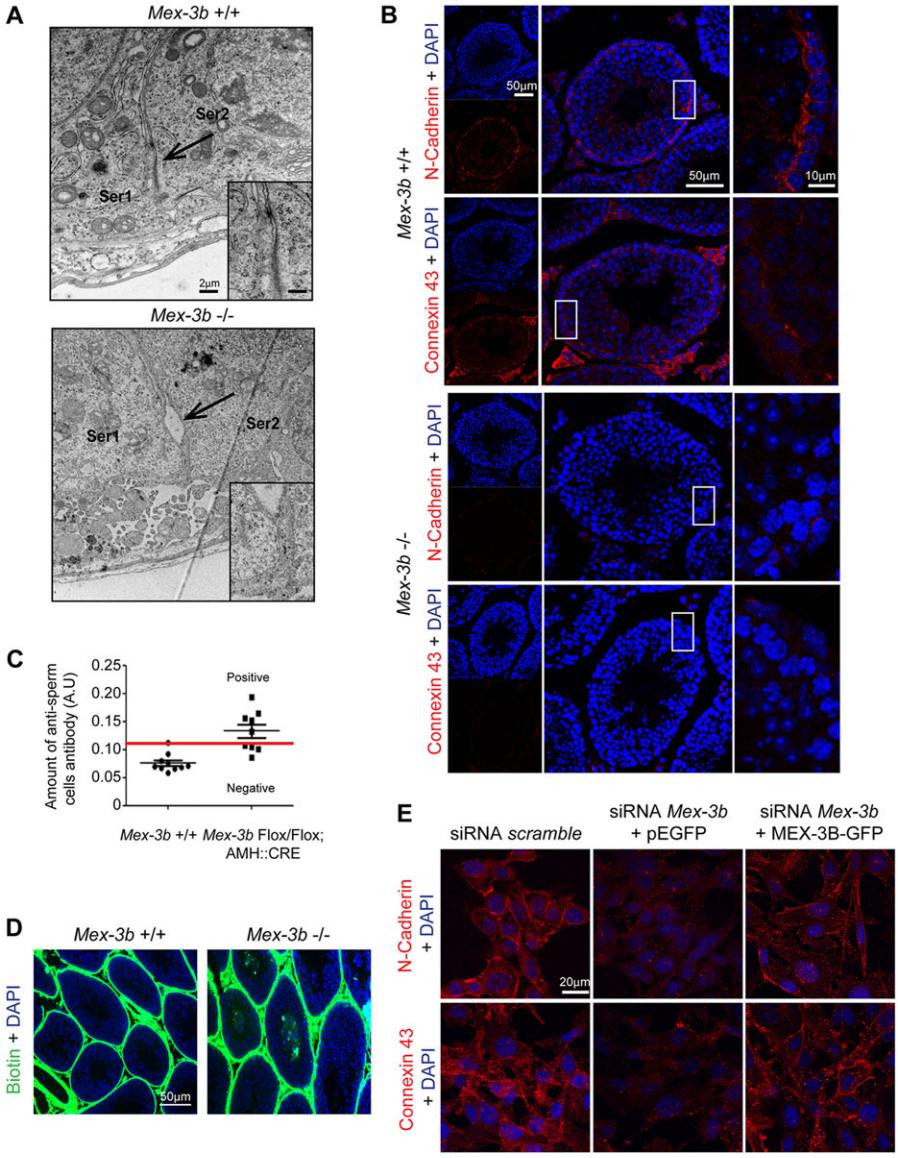

Fig. 4. Mex3b controls adhesion properties of Sertoli cells. (A) Electron microscopy images of intercellular junctions in testes sections from wild-type and *Mex3b*-deficient mice. Arrows indicate cellular junctions constituting the BTB between two adjacent Sertoli cells (Ser1 and Ser2). Insets show magnification of the cellular junction region. Scale bars in insets: 60 nm. (B) Confocal microscope images of wild-type and *Mex3b*-deficient mice testis sections immunostained for N-cadherin and connexin 43 (red) (6-month-old mice). DAPI was used to stain nuclei and white boxes indicate the area magnified in the inserts. (C) Detection of anti-sperm cell antibodies in serum of wild-type and *Mex3b*$^{Flox/Flox}$*; AMH::Cre*-deficient mice. Red line indicates the limit of ELISA test's significance according to the manufacturer (threshold of test positivity). (D) Epifluorescence images of sections from adult wild-type and *Mex3b*-deficient mice testis, previously injected with a biotin tracer that was allowed to diffuse in the seminiferous tubes of living mice for 30 min. (E) Confocal microscope images of TM4 cells with endogenous *Mex3b* inhibited by siRNA and re-expressing the human MEX3B protein. N-cadherin and connexin 43 (red) were immunostained and counterstained with DAPI.

intercellular spaces between adjacent cells. The inset in Fig. 4A shows focal disruption of the BTB, thus confirming that the barrier integrity was severely compromised in *Mex3b*$^{-/-}$ seminiferous tubules.

Then, we examined the expression of N-cadherin (N-Cad; Cdh2 – Mouse Genome Informatics) and connexin 43 (Cx43; Gja1 – Mouse Genome Informatics), two molecules that contribute to the formation of the BTB and are constituent proteins of adherens and gap junctions, respectively (Li et al., 2010; Newton et al., 1993). Immunofluorescence staining of the wild-type mouse seminiferous epithelium with antibodies recognizing these two proteins identified a belt-like structure near the basal lamina that corresponds to the BTB (Fig. 4B). By contrast, the labeling of N-Cad and Cx43 was weaker and more diffuse in the *Mex3b* knockout mice seminiferous tubules (Fig. 4B).

Abnormal permeability of the BTB may result in the release of germ cells in the bloodstream that leads to the mounting of an autoimmune response and the production of anti-sperm antibodies. Therefore, we measured the level of anti-sperm antibodies in the serum of mice with a genetic disruption of *Mex3b* in Sertoli cells. As shown in Fig. 4C, anti-sperm antibodies were detected in the serum of mice deficient for *Mex3b* in Sertoli cells at a level that was higher than the limit of the test positivity, in contrast to observations in the wild-type mouse. Consistently, a biotin marker injected under the testicular tunica albuginea of *Mex3b* knockout mice was able to diffuse in the lumen of seminiferous tubules in a reproducible manner, whereas it was blocked by the intact BTB of wild-type mice (Fig. 4D). These data confirm that the tightness of the BTB was weakened in *Mex3b*-deficient seminiferous tubules.

Finally, to reinforce these data, we studied N-Cad and Cx43 expression in TM4 cells knocked down for Mex3b. Staining of these two intercellular junction components decorated the surface of TM4 cells, whereas this labeling was lost upon silencing of *Mex3b* (Fig. 4E). Expression of MEX3B-GFP restored N-Cad and Cx43 localization at the plasma membrane of Mex3b knockdown TM4 cells. To test whether the overall mRNA and protein levels of Cx43 and N-Cad were affected by the loss of Mex3b, their expression were assessed by qPCR and western blot (supplementary material Fig. S4D,F), showing a decrease of mRNA expression for both Cx43 and N-Cad as well as a reduction in the protein level of Cx43. These results indicate that Mex3b modulates both the expression and the localization of these two junction proteins.

Development (2014) 141, 2096-2107 doi:10.1242/dev.108514

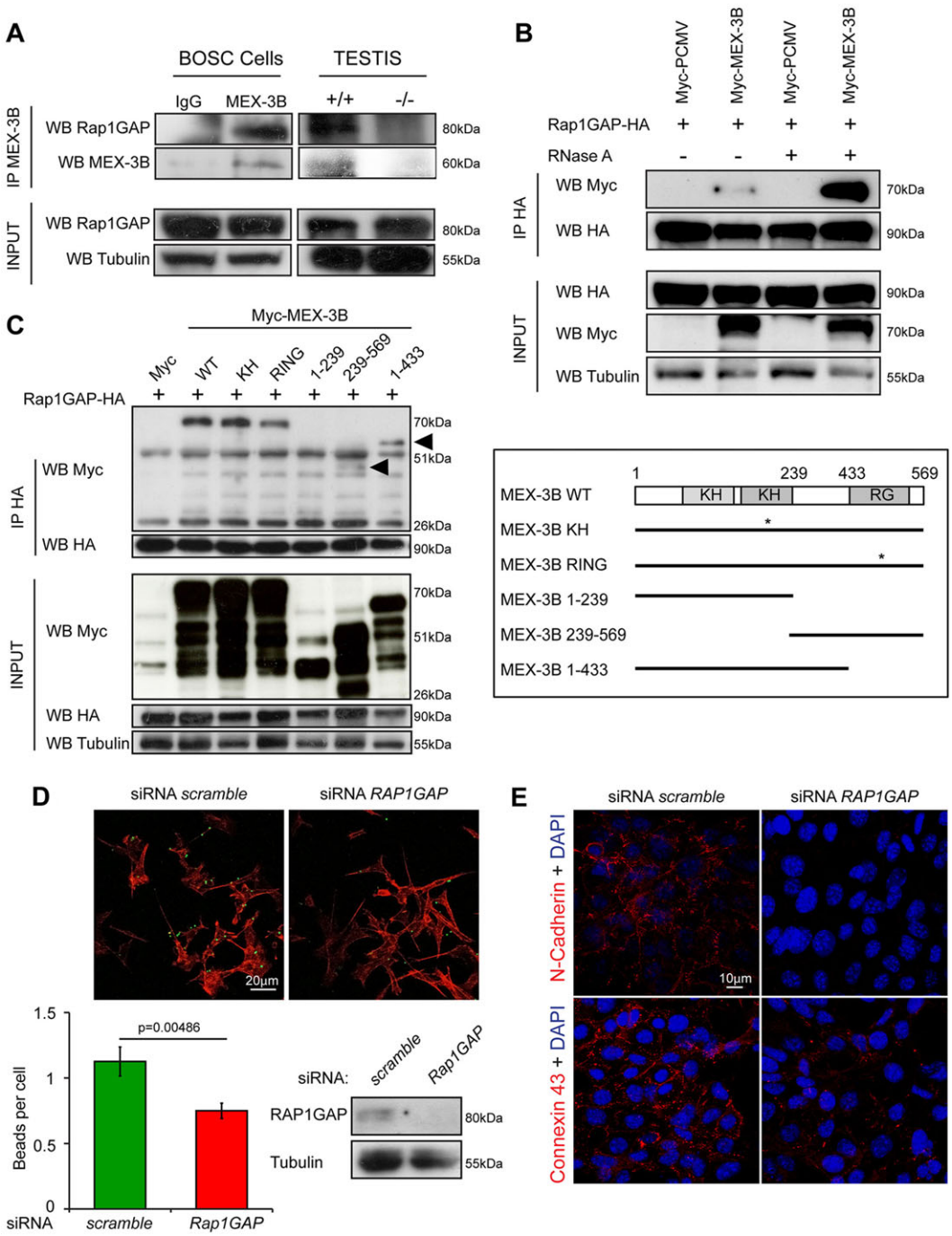

Fig. 5. Mex3b functionally interacts with Rap1GAP. (A) Endogenous interaction between MEX3B and Rap1GAP assessed by immunoprecipitation from human epithelial BOSC cells and whole mouse testis lysates. (B) Immunoprecipitation of Myc-MEX-3B and Rap1GAP-HA after RNase A treatment of the cell lysates. Immunoprecipitation of HA-tag and detection with Myc, HA and tubulin antibodies are shown. (C) BOSC cells were transfected with plasmids expressing Rap1GAP-HA and Myc-MEX-3B constructs as depicted in the right-hand panel. Point mutations in different domains are represented by an asterisk. Left-hand panel shows immunoprecipitation with the anti-HA tag antibody followed by western blot analysis using Myc, HA and tubulin antibodies. Immunoprecipitated MEX3B mutants are indicated by black arrowheads. Blots are representative of three independent experiments. (D) TM4 cells treated with scramble or *Rap1GAP* siRNA were incubated with latex beads (pseudocolored in green), fixed and stained with phalloidin-TRITC before observation under epifluorescent microscope (top panel). Histograms (bottom left panel) indicate the average number of phagocytosed fluorescent beads per phalloidin-TRITC stained cell (n=200 cells per condition). Western blot analysis of Rap1GAP levels after siRNA knockdown in TM4 cells (bottom right panel). Error bars represent s.e.m. (E) N-cadherin and connexin 43 localization were assessed after siRNA *Rap1GAP* treatment by immunofluorescence using confocal microscopy. TM4 cells were counterstained with DAPI.

Mex3b interacts with Rap1GAP

While exploring possible mechanisms accounting for the role of Mex3b in phagocytosis and in intercellular adhesion, our attention was drawn to a large-scale yeast two-hybrid screen that found that the GTPase-activating protein Rap1GAP binds to MEX3B (Stelzl et al., 2005). Rap1 is a small GTP-binding protein that cycles between an active, GTP-bound, and an inactive, GDP-bound state (Caron, 2003; Gloerich and Bos, 2011). Interestingly, Rap1 proteins

Development (2014) 141, 2096-2107 doi:10.1242/dev.108514

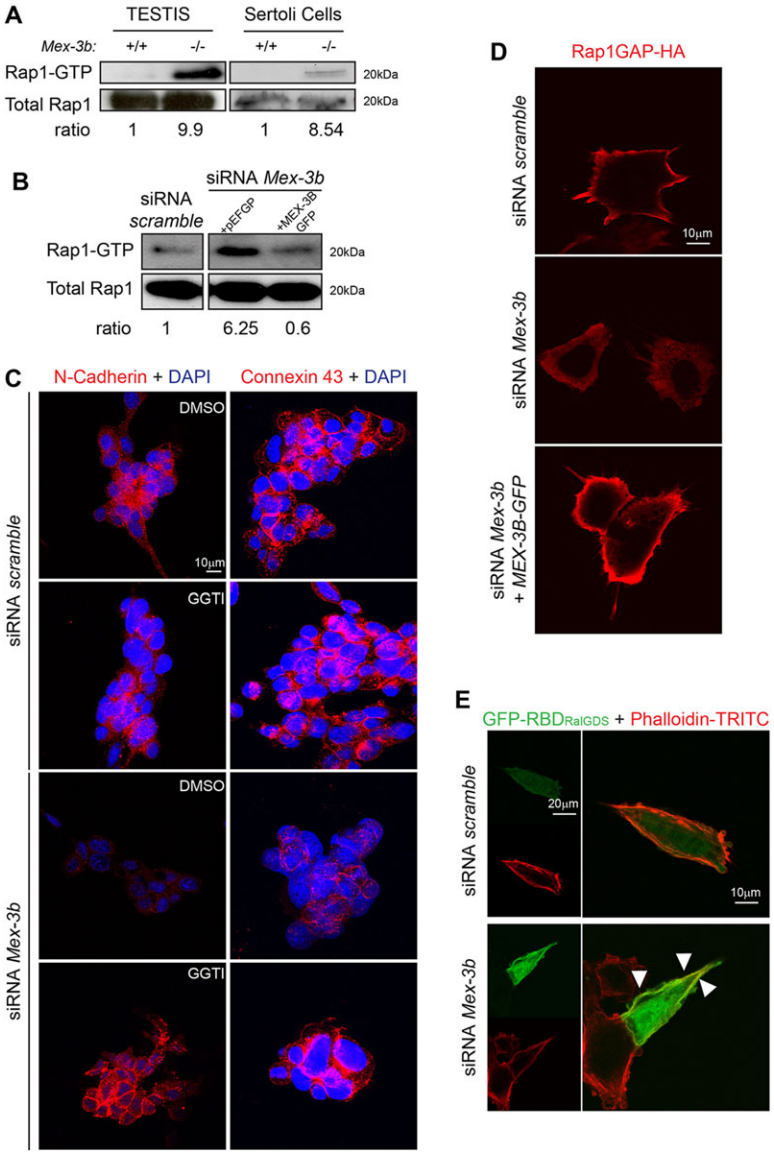

Fig. 6. Mex3b regulates Rap1 activity through the recruitment of Rap1GAP at the plasma membrane. (A) Rap1-GTP pulldown from whole testis and purified Sertoli cells lysates assessed by western blot. The ratio of Rap1-GTP/Total Rap1 for each condition is indicated underneath the western blot. (B) Rap1-GTP pulldown from lysates of TM4 cells treated with siRNA targeting mouse *Mex3b* mRNA and re-expressing human MEX3B-GFP protein. (C) N-cadherin and connexin 43 localization after siRNA and GGTI-298 treatment was visualized by immunofluorescence using confocal microscopy. Cells were counterstained with DAPI. (D) Immunolocalization of Rap1GAP-HA in TM4 cells knocked down for Mex3b expression by siRNA and re-expressing MEX3B-GFP after serum stimulation. (E) Localization of GFP-RBD_{ralGDS} in TM4 cells knocked down for Mex3b expression by siRNA. Cells were exposed to phalloidin-TRITC prior to observation by confocal microscopy. White arrowheads indicate the accumulation of GFP-RBD_{ralGDS}.

are key regulators of phagocytosis and cell-cell adhesion. Rap1GAP, the putative MEX3B interactor, belongs to a group of related molecules which increase the intrinsic GTPase activity of Rap1, thereby antagonizing the function of Rap1 guanine nucleotide exchange factors (Rap1-GEFs) that load GTP on Rap1 (Polakis et al., 1991; Rubinfeld et al., 1991).

We first examined whether endogenous MEX3B and Rap1GAP proteins interacted in cells. Immunoprecipitation of the endogenous human MEX3B from a lysate of human kidney epithelial cells (BOSC cells) followed by a western blot with an anti-Rap1GAP antibody revealed a specific interaction between these two molecules (Fig. 5A). The complex between endogenous Mex3b and Rap1GAP was also detected in mouse *Mex3b*$^{+/+}$ testis extracts and, as expected, no Rap1GAP was co-immunoprecipitated with the polyclonal serum recognizing MEX3B when testis extracts were prepared from the *Mex3b*$^{-/-}$ mice (Fig. 5A). As RBPs may indirectly bind to another protein through RNA bridging, we expressed epitope-tagged Myc-MEX-3B and Rap1GAP-HA and incubated transfected BOSC cell extracts with RNase A after lysis. As shown in Fig. 5B, the complex between Myc-MEX-3B and Rap1GAP-HA did not dissociate upon RNase A treatment, but, on the contrary, the binding between these two proteins was even slightly strengthened under this condition. Thus, our data confirm that MEX3B and Rap1GAP physically interact in an RNA-independent manner.

In order to map the regions of MEX3B involved in Rap1GAP binding, we constructed a series of Myc-tagged *MEX3B* deletion mutants. Immunoblotting with the anti-HA and anti-Myc antibodies confirmed that Rap1GAP-HA and mutants Myc-MEX-3B were expressed at similar levels after transfection (Fig. 5C). As shown in Fig. 5C, deletion of the first 239 amino acids (MEX-3B 239-569 mutant) did not abolish this interaction whereas truncation of MEX3B after the second KH domain (MEX-3B 1-239) prevented the binding of Rap1GAP-HA. Together, these data show that Rap1GAP interaction surface of MEX3B encompasses the region between the second KH domain and the ring finger motif.

We next wondered whether phagocytic and adhesion defects observed in *Mex3b*-depleted cells could be linked to the effect on Rap1GAP and the Rap1 pathway. If this hypothesis is true, the silencing of *Rap1GAP* in TM4 cells should phenocopy the lack of *Mex3b*. Using this approach, we found that Rap1GAP knockdown resulted in the reduction of both phagocytosis (Fig. 5D) and of N-Cad

Development (2014) 141, 2096-2107 doi:10.1242/dev.108514

and Cx43 at the cell surface, a phenotype that was comparable to what was observed when Mex3b expression was downregulated (Fig. 5E). Furthermore, expression of a truncated version of MEX3B unable to bind RAP1GAP (MEX-3B 1-239) in TM4 cells previously knocked down for *Mex3b* did not restore membrane localization of N-cadherin and connexin 43 as full-length MEX3B did (Fig. 4E; supplementary material Fig. S5). Altogether, these data are consistent with a positive coupling between MEX3B and Rap1GAP in the regulation of phagocytosis and cell-cell interaction.

Mex3b regulates the activity and the spatial localization of Rap1GAP

Mex3b interaction with Rap1GAP might impact its ability to modulate Rap1 activity. Thus, to determine whether Mex3b could regulate Rap1 activity, we performed a series of pulldown assays to precipitate GTP-bound Rap1 using the Rap1 substrate Ral-GDS (van Triest et al., 2001). A robust and reproducible increase of Rap1-GTP was observed in $Mex3b^{-/-}$ testis extracts compared with the $Mex3b^{+/+}$ control (Fig. 6A). A similar enhancement of Rap1-GTP was revealed in $Mex3b^{-/-}$ primary cultures of Sertoli cells compared with $Mex3b^{+/+}$ Sertoli cells (Fig. 6A). We further confirmed these data in TM4 cells after *Mex3b* silencing. In addition, expression of human MEX3B in TM4 cells treated with siRNA targeting mouse *Mex3b* reduced the level of Rap1-GTP to that observed in TM4 cells transfected with scrambled siRNA (Fig. 6B) without modification of Rap1GAP RNA or protein levels (supplementary material Fig. S4D,E). Thus, we conclude that Mex3b positively regulates Rap1GAP function and thereby restrains Rap1 activity.

As *Mex3b* depletion reduces intercellular adhesion and regulates the activity of Rap1 through Rap1GAP, we tested whether the effect of Mex3b on cell-cell contact was dependent on Rap1 activation. We speculated that a mild reduction of Rap1 signaling could rescue the proper localization of N-Cad and Cx43 at the cell surface. To test this idea, *Mex3b* was silenced in TM4 cells and exposed to the Rap1 inhibitor GGTI-298 (Efuet and Keyomarsi, 2006). Analysis of Rap1-GTP levels by pulldown confirmed the partial inhibition of Rap1 activity after 30 min of exposure to 12.5 µM GGTI (supplementary material Fig. S6A). As shown in Fig. 6C, this treatment led to the redistribution of N-Cad and Cx43 to the cell surface in TM4 cells knocked down for Mex3b. Thus, a sustained activation of Rap1 subsequent to the loss of Mex3b is responsible for the failure of N-Cad and Cx43 to be localized and stabilized at the cell surface.

It has been previously reported that the spatial gradient of Rap1-GTP depends on Rap1GAP activity, which is higher in the periphery than in the central region of the cells (Mochizuki et al., 2001; Ohba et al., 2003). These results prompted us to examine whether Mex3b could regulate Rap1GAP subcellular localization. As previously described (Buchet-Poyau et al., 2007), exogenously expressed MEX3B-GFP fusion is localized in the nucleus, in the cytoplasm and also decorates the cell cortex (supplementary material Fig. S6B). Accordingly, an epitope-tagged Rap1GAP-HA construct localizes to the cortical plasma membrane of TM4 cells under serum stimulation (Fig. 6D). Strikingly, *Mex3b* silencing perturbed this cortical localization and led to a more diffuse cytoplasmic pattern. Furthermore, re-expression of MEX3B in Mex3b knocked down cells restored Rap1GAP-HA localization to the plasma membrane (Fig. 6D). These results indicate that Mex3b is required for the proper targeting of Rap1GAP to the inner face of the plasma membrane.

To address this hypothesis directly, we used the fusion protein GFP-RBD_{RalGDS}, which interacts with Rap1-GTP and allows the visualization of active Rap1 through GFP signal (Bivona et al., 2004). Under control conditions, Rap1-GTP was detected in the cytoplasm and was weakly enriched at the plasma membrane of TM4 cells in basal conditions (Fig. 6E). However, upon silencing of *Mex3b*, we observed a marked increase of the GFP signal with a clear enhancement of the labeling at the plasma membrane, thus reflecting a higher Rap1-GTP concentration at the cell cortex. Furthermore, GGTI treatment reduced the overall GFP signal and clearly diminished the decoration of the inner face of the plasma membrane with the GFP-RBD_{RalGDS} (supplementary material Fig. S6C). Overall, these results indicate that Mex3b regulates the expression of intercellular adhesion molecules by controlling the level and the localization of Rap1-GTP via its effect on both Rap1GAP activity and transport.

DISCUSSION

We report here that *Mex3b*-deficient mice are subfertile. Investigation of the pathophysiological processes in *Mex3b*-deficient males showed that residual bodies released by spermatids during their differentiation obstruct a fraction of mouse seminiferous tubules, thus causing a net decrease in the spermatozoa yield. In addition, the BTB is loosened and anti-sperm antibodies are produced. These effects were found to arise from a disruption of phagocytosis and adhesive abilities of *Mex3b*-deficient Sertoli cells. Exploration of the underlying mechanisms revealed the causative role of a sustained activation of Rap1 at the Sertoli cell cortex that is a consequence of a perturbation of Rap1GAP function, activity and subcellular localization of which are controlled by Mex3b. Thus, this work unveils a key role for Mex3b in the spatial organization of the Rap1 signaling pathway, which regulates Sertoli cell biological properties.

Our results indicate that a third of seminiferous tubules was obstructed in *Mex3b* null mice testes and a similar proportion of tubules was affected in males with a *Mex3b* locus specifically disrupted in Sertoli cells. This incomplete penetrance could be linked to the modifying effects of the genetic makeup of the mice, but we cannot formally exclude a compensatory effect of other Mex3 genes that are expressed in Sertoli cells. We also observed that the multilayers of granulosa cells surrounding the oocyte showed an abnormal histology in $Mex3b^{-/-}$ female ovaries. As granulosa cells share the same embryonic origin than Sertoli cells and communicate via gap junctions containing Cx43 (Patek et al., 1991), it is possible that Mex3b regulates granulosa functions and folliculogenesis through the same mechanisms identified in Sertoli cells.

It is well documented that Sertoli cells have a key scavenger function as they eliminate apoptotic germ cells and remove residual bodies released during the cytoplasmic reduction phase of spermiogenesis (Nakanishi and Shiratsuchi, 2004). However, we did not notice a decrease in the clearance of apoptotic germ cells in *Mex3b* null mice. Spermiation occurs at the apical adluminal compartment of the tubules, which contains round elongating/elongated spermatids attached to Sertoli cells via an actin-based adherens junction (AJ) type designated as the apical ectoplasmic specialization (ES) (Lee and Cheng, 2004). Thus, *in vivo*, the action of Mex3b may be compartmentalized to this region of the Sertoli-germ cell interface to control phagocytic removal of residual bodies, a question that remains to be explored. Although we did not observe an overt reduction of $Mex3b^{-/-}$ sperm cell motility, we cannot formally exclude that this Sertoli phagocytic defect may also affect spermiogenesis and consequently decrease the sperm fertilizing fitness.

A net reduction of N-Cad and Cx-43, two junction molecules that contribute to the establishment of the BTB, is observed in the

Development (2014) 141, 2096-2107 doi:10.1242/dev.108514

seminiferous tubules of *Mex3b*-deficient mice. Consistently, electron microscopy analysis shows a focal disruption of the BTB in the *Mex3b*$^{-/-}$ testis and experiments using a biotin tracer confirm that the tightness of the BTB is indeed altered. The detection of anti-sperm antibodies in the serum of mice deficient for *Mex3b* in Sertoli cells convincingly strengthens the notion that the integrity of the BTB is impaired in the absence of *Mex3b*.

Our conclusion that Mex3b is a regulator of the Rap1 pathway involved in BTB formation is based on the following series of complementary results: (1) endogenous Mex3b binds to Rap1GAP; (2) *Mex3b* inactivation in mouse prevents Rap1GAP localization at the cell cortex and leads to aberrant Rap1 activation as revealed by biochemical approaches and imaging techniques that identify Rap1-GTP in cells; (3) the membrane localization of N-Cad and Cx43 depends on the ability of Mex3b to bind Rap1GAP and treatment of TM4 cells deficient for *Mex3b* with the Rap1 inhibitor GGTI-298 rescues the proper cell surface expression of these two cell junction molecules; and finally, (4) *Rap1GAP* RNAi phenocopies the phagocytosis and cell-cell interactions defects generated by the lack of *Mex3b*. Thus, these data, together with the observed diminution of the levels of *N-Cad* and *Cx43* transcripts in the absence of *Mex3b*, raise the idea that this RBP acts at successive steps to regulate the proper expression of these junction molecules at the cell surface: (1) in the post-transcriptional stabilization of *N-Cad* and *Cx43* transcripts, possibly involving the direct binding of Mex3b on these mRNAs; and (2) in the spatial control of the Rap1 pathway to achieve the appropriate localization and stabilization of these adhesion molecules at the plasma membrane.

In macrophages, activation of Rap1 has been reported to promote phagocytosis of opsonized targets in macrophages (Caron et al., 2000). However, our study indicates that an aberrant activation of Rap1 at the cell cortex is responsible for the loss of phagocytic capacity of Sertoli cells. Consistently, activation of Rap1 has also been shown to suppress phagocytosis of polystyrene beads by microglial cells (Steininger et al., 2011). Thus, it is possible that the contribution of the Rap1 pathway in phagocytosis depends on the nature of the particles engulfed and also on the cell type involved.

Rap1GAP activity has been found to be higher at the plasma membrane and the preferential localization of this protein is believed to contribute to the establishment of an intracellular gradient of Rap1-GTP (Ohba et al., 2003). Furthermore, the Rap1GAP ortholog Bud2 in *Saccharomyces cerevisiae* is targeted to the membrane of the incipient bud through interaction with proteins that specify the cortical landmark where it constitutes with Rsr1/Rap1 and Bud5/Rap1GEF, the module that positions the bud formation at a particular site (Park and Bi, 2007). Even more relevant to this topic, Rap1 (Roughened – FlyBase) signaling in a group of somatic cells of *Drosophila* testes, called the hub, controls stem cell anchoring via the appropriate positioning of DE-cadherin (Shotgun – FlyBase) at the interface between these cell types (Wang et al., 2006). Our findings are fully consistent with these results and further reveal a novel level of regulation with Mex3b mediating the localization of Rap1GAP to the plasma membrane. However, the underlying mechanisms remain to be determined. It is possible that Mex3b, associated or not with target RNAs, binds directly to the cytoskeleton or to cytoskeletal motors ferrying the Mex3b-Rap1GAP complex to the cell cortex. The contribution of long non-coding (lnc)RNA in the stabilization and the transport of the Mex3b-Rap1GAP complex merits exploration in view of the recent demonstration that the lncRNA *HOTAIR* binds to MEX3B (Yoon et al., 2013).

In conclusion, this study provides insights into the *in vivo* function of mammalian MEX-3 proteins by ascribing a role to Mex3b in the spatial assembly of the Rap1 pathway, which proves necessary for normal Sertoli cell physiology. This work is congruent with recent large-scale analyses that discovered a general scaffolding role for RBPs in the dynamic organization of localized signaling centers (de Hoog et al., 2004; Lécuyer et al., 2007). As alterations of the integrity of the BTB is a frequent cause of male infertility, it is plausible that mutations affecting either *MEX3B* or genes coding for components of the Rap1 pathway may account for cases of human spermatogenic defects.

MATERIALS AND METHODS

Mice

Total and Sertoli cell-specific *Mex3b* null mice were generated using embryonic stem cell technology as described (Hogan et al., 1994). For details of generation and genotyping, see supplementary materials and methods.

All animal experiments were conducted according to the standard ethical guidelines of the Institut National de la Santé et de la Recherche Médicale (INSERM).

Reproductive ability of mice was assessed by mating 2-month-old mice of the indicated genotype for 9 months. For the counting of sperm cells, caudae epididymidis and vasa deferentia were excised. Semen was allowed to exude for 15 min at 37°C and counted using a Malassez grid.

Cell lines

MEFs were isolated from E12.5 embryos as previously described. Sertoli cells were isolated from ∼10- to 14-day-old mice and cultured as described previously (Weiss et al., 1997). The mouse TM4 Sertoli and human BOSC cell lines were obtained from the American Tissue Culture Collection (ATCC).

Phagocytosis assay

Monolayers of cells were incubated with 2-µm diameter carboxylate-modified FluoSpheres (Invitrogen) for 2 hours at 37°C with a ratio of 40 beads per cell (adapted from Park et al., 2007). *z*-stack acquisitions were performed using a biphotonic confocal microscope (LSM510 META NLO). The number of beads per cells was determined by counting random fields on the glass with LSM image browser software.

Western blot and immunoprecipitation

Cells were lysed 48 h post-transfection and immunoprecipitation and western blot analyses were performed as described previously (Nony et al., 2003). When indicated, protein extracts were treated with RNAse A (0.2 mg/ml; Roche) prior to immunoprecipitation. When performed, Rap1 activation assay was carried out according to the manufacturer's protocol (Rap1 activation assay kit; Millipore) and quantification of Rap1-GTP/total Rap1 was performed using ImageJ software.

Antibodies and reactives

Mouse monoclonal anti-myc (9E10), anti-GFP (Roche Applied Science), anti-HA (16B12, Covance), anti-tubulin (gift from L. Lafanachère, INSERM, U823; Université Joseph Fourier-Grenoble; Institut Albert Bonniot, Grenoble F-38700, France), and anti-Rap1GAP (H-93, Santa Cruz Biotechnology) antibodies were used in western blots at 1:5000, 1:1000, 1:1000, 1:250,000 and 1:1000, respectively. Rabbit polyclonal anti-Mex3b antibody was used for western blots at 1:750 and recognizes both mouse and human Mex3b. Rap-1 inhibitor GGTI-298 was purchased from Sigma-Aldrich.

Histological sections, immunofluorescence staining and electron microscopy

Tissues samples were placed in 4% formaldehyde or Alcoholic Bouin's overnight and embedded in paraffin or directly frozen at −80°C. For details of staining, see supplementary materials and methods.

After the staining, vimentin-positive cells (Sertoli cells) were counted as well as germ cells with the Hematoxylin counterstain in seminiferous tubules. For stages I-VII, all round spermatids were counted and for stages VII-XII, all pachytene spermatocytes were numerated based on the established classification of seminiferous tubules staging (Russell and Peterson, 1985) (n=100 seminiferous tubules on six male mice at each age point).

Development (2014) 141, 2096-2107 doi:10.1242/dev.108514

Immunofluorescence analyses on frozen section and cells were performed as described previously (Carette et al., 2010). N-cadherin, connexin 43 and 15-lipoxygenase (gift from P. Sutovsky, University of Missouri, Columbia, USA) antibodies were used at 1:100. Immunolocalization of Rap1GAP-HA and human MEX3B-GFP protein was determined after overnight deprivation of serum and a short activation (10 min).

For electron microscopy, testis pieces were fixed with glutaraldehyde, post-fixed in reduced osmium, dehydrated and embedded in Epon as previously described (Lablack et al., 1998). The sections were analyzed with a JEOL 1200EX electron microscope (Institut des Neurosciences, Grenoble, France).

Detection of anti-sperm cell antibodies

Sperm antibodies were measured in the serum of 3-month-old wild-type and *Mex3b*$^{Flox/Flox}$*; AMH::Cre* deficient mice using the ELISA kit from Cusabio as specified by the manufacturer's instructions.

Biotin tracer studies

The permeability of the BTB was assessed by using a biotin tracer as described previously (Meng et al., 2005). For details, see supplementary materials and methods.

Cloning and transfection

Myc-Mex-3b and Myc-Mex-3b mutants were cloned in Myc-pCMV-Tag3B vector (Stratagene) as described previously (Buchet-Poyau et al., 2007). pmT2/Rap1GAP-HA and GFP-RBD$_{RalGDS}$ (gift from R. Philips, University of North Carolina, Chapel Hill, USA) constructs were also used. For the rescue experiments, pLENTI CAG-human MEX3B fused with GFP were designed to infect TM4 cells and ensure that siRNA against mouse *Mex3b* did not reduce expression of human MEX3B-GFP.

Short interfering RNAs (siRNAs) against the mouse *Mex*3b and *Rap1GAP* gene and the non-targeting control siRNA were purchased from Dharmacon (ON-TARGET plus SMART pool RKHD3 ref. L-056400-01-0020 and ON-TARGET plus Non-targeting Pool ref. D-001810-10-05, Dharmacon). siRNAs were transfected into TM4 cells using Lipofectamine 2000 RNAi max (Invitrogen) following the manufacturer's protocol. For details of transfection and infection, see supplementary materials and methods.

RNA isolation and RT-PCR analysis

Total RNA was extracted from cell lines or tissues using the RNeasy Mini Kit (Qiagen) according to the manufacturer's instructions. Then, RNAs were reverse transcribed to cDNA using the Omniscript Reverse Transcription Kit (Qiagen) and real-time RT-PCR was performed using the MXP-3000P PCR-system (Stratagene). RNA of pachytene spermatocytes (PS) or round spermatids (RS) were obtained by centrifugal elutriation.

The sequences of the different primers used for RT-PCR are listed in supplementary material Table S1.

Statistical analysis

All experiments were carried out in triplicate or with a significant number of individuals and statistical analyses were performed with the statistical package GraphPad Prism using the unpaired Student's *t*-test (confidence intervals 99%). Values are given as mean and standard error of the mean (s.e.m.).

Acknowledgements

We thank Hervé Le Hir, Kiran Padmanabhan, Karin Sadoul and André Verdel for critical reading of the manuscript. We thank Peter Sutovsky for the kind gift of the polyclonal serum anti-15-LOX; Mark R. Philips for the kind gift of the vector expressing the GFP-RBD$_{RalGDS}$; and Gisèle Froment and Caroline Costa from the lentivectors production facility (SFR BioSciences Gerland–Lyon Sud UMS3444/US8).

Competing interests

The authors declare no competing financial interests.

Author contributions

M.L.B., K.B.-P., N.C., J.C. and M.B. conceived and designed the experiments. M.L.B., K.B.-P., C.T. and N.C. performed a large part of the experiments from mouse phenotyping to molecular biology studies. O.D., E.F. and C.A.-R. contributed to biochemistry and imaging experiments. J.-P.R. engineered the lentiviral vectors expressing MEX3 proteins and D.N. produced lentiviral particles. D.S. contributed to the interpretation of the electron microscopic images. S.R. and S.K. discussed regularly the results concerning the fertility phenotype, suggested experiments and shared protocols and expertise. D.B., P.C. and F.G. participated to the generation of the mouse models. P.D. and M.-H.P. were involved in the characterization of the testis phenotype, in the primary culture of Sertoli cells and in the phagocytosis assays. M.B., M.L.B. and N.C. wrote the manuscript.

Funding

This work was supported by a grant from the Association pour la Recherche sur le Cancer (ARC) [20110603000]; a fellowship from ARC (to M.L.B.); and a fellowship from the Fondation Pour la Recherche Médicale (FRM) (to N.C.).

Supplementary material

Supplementary material available online at
http://dev.biologists.org/lookup/suppl/doi:10.1242/dev.108514/-/DC1

References

Baltz, A. G., Munschauer, M., Schwanhäusser, B., Vasile, A., Murakawa, Y., Schueler, M., Youngs, N., Penfold-Brown, D., Drew, K., Milek, M. et al. (2012). The mRNA-bound proteome and its global occupancy profile on protein-coding transcripts. *Mol. Cell* **46**, 674-690.

Betz, U. A. K., Vosshenrich, C. A. J., Rajewsky, K. and Müller, W. (1996). Bypass of lethality with mosaic mice generated by Cre-loxP-mediated recombination. *Curr. Biol.* **6**, 1307-1316.

Bivona, T. G., Wiener, H. H., Ahearn, I. M., Silletti, J., Chiu, V. K. and Philips, M. R. (2004). Rap1 up-regulation and activation on plasma membrane regulates T cell adhesion. *J. Cell Biol.* **164**, 461-470.

Boussouar, F. and Benahmed, M. (2004). Lactate and energy metabolism in male germ cells. *Trends Endocrinol. Metab.* **15**, 345-350.

Buchet-Poyau, K., Courchet, J., Le Hir, H., Séraphin, B., Scoazec, J.-Y., Duret, L., Domon-Dell, C., Freund, J.-N. and Billaud, M. (2007). Identification and characterization of human Mex-3 proteins, a novel family of evolutionarily conserved RNA-binding proteins differentially localized to processing bodies. *Nucleic Acids Res.* **35**, 1289-1300.

Burrell, R. A.,, McClelland, S. E., Endesfelder, D., Groth, P., Weller, M.-C., Shaikh, N., Domingo, E., Kanu, N., Dewhurst, S. M., Gronroos, E. et al. (2013). Replication stress links structural and numerical cancer chromosomal instability. *Nature* **494**, 492-496.

Cano, F., Bye, H., Duncan, L. M., Buchet-Poyau, K., Billaud, M., Wills, M. R. and Lehner, P. J. (2012). The RNA-binding E3 ubiquitin ligase MEX-3C links ubiquitination with MHC-I mRNA degradation. *EMBO J.* **31**, 3596-3606.

Carette, D., Weider, K., Gilleron, J., Giese, S., Dompierre, J., Bergmann, M., Brehm, R., Denizot, J.-P., Segretain, D. and Pointis, G. (2010). Major involvement of connexin 43 in seminiferous epithelial junction dynamics and male fertility. *Dev. Biol.* **346**, 54-67.

Caron, E. (2003). Cellular functions of the Rap1 GTP-binding protein: a pattern emerges. *J. Cell Sci.* **116**, 435-440.

Caron, E., Self, A. J. and Hall, A. (2000). The GTPase Rap1 controls functional activation of macrophage integrin alphaMbeta2 by LPS and other inflammatory mediators. *Curr. Biol.* **10**, 974-978.

Castello, A., Fischer, B., Eichelbaum, K., Horos, R., Beckmann, B. M., Strein, C., Davey, N. E., Humphreys, D. T., Preiss, T., Steinmetz, L. M. et al. (2012). Insights into RNA biology from an atlas of mammalian mRNA-binding proteins. *Cell* **149**, 1393-1406.

Cheng, C. Y. and Mruk, D. D. (2012). The blood-testis barrier and its implications for male contraception. *Pharmacol. Rev.* **64**, 16-64.

Ciosk, R., DePalma, M. and Priess, J. R. (2006). Translational regulators maintain totipotency in the Caenorhabditis elegans germline. *Science* **311**, 851-853.

Courchet, J., Buchet-Poyau, K., Potemski, A., Brès, A., Jariel-Encontre, I. and Billaud, M. (2008). Interaction with 14-3-3 adaptors regulates the sorting of hMex-3B RNA-binding protein to distinct classes of RNA granules. *J. Biol. Chem.* **283**, 32131-32142.

de Hoog, C. L., Foster, L. J. and Mann, M. (2004). RNA and RNA binding proteins participate in early stages of cell spreading through spreading initiation centers. *Cell* **117**, 649-662.

Donnini, M., Lapucci, A., Papucci, L., Witort, E., Jacquier, A., Brewer, G., Nicolin, A., Capaccioli, S. and Schiavone, N. (2004). Identification of TINO: a new evolutionarily conserved BCL-2 AU-rich element RNA-binding protein. *J. Biol. Chem.* **279**, 20154-20166.

Draper, B. W., Mello, C. C., Bowerman, B., Hardin, J. and Priess, J. R. (1996). MEX-3 is a KH domain protein that regulates blastomere identity in early C. elegans embryos. *Cell* **87**, 205-216.

Efuet, E. T. and Keyomarsi, K. (2006). Farnesyl and geranylgeranyl transferase inhibitors induce G1 arrest by targeting the proteasome. *Cancer Res.* **66**, 1040-1051.

Fischer, K. A., Van Leyen, K., Lovercamp, K. W., Manandhar, G., Sutovsky, M., Feng, D., Safranski, T. and Sutovsky, P. (2005). 15-Lipoxygenase is a component of the mammalian sperm cytoplasmic droplet. *Reproduction* **130**, 213-222.

Gloerich, M. and Bos, J. L. (2011). Regulating Rap small G-proteins in time and space. *Trends Cell Biol.* **21**, 615-623.

Hogan, B., Beddington, R., Costantini, F. and Lacy, E. (1994). *Manipulating the Mouse Embryo: A Laboratory Manual*, pp. 311e5. Cold Spring Harbor, New York: CSH Press.

Hogan, D. J., Riordan, D. P., Gerber, A. P., Herschlag, D. and Brown, P. O. (2008). Diverse RNA-binding proteins interact with functionally related sets of RNAs, suggesting an extensive regulatory system. *PLoS Biol.* **6**, e255.

Hunter, C. P. and Kenyon, C. (1996). Spatial and temporal controls target pal-1 blastomere-specification activity to a single blastomere lineage in C. elegans embryos. *Cell* **87**, 217-226.

Jabado, N., Canonne-Hergaux, F., Gruenheid, S., Picard, V. and Gros, P. (2002). Iron transporter Nramp2/DMT-1 is associated with the membrane of phagosomes in macrophages and Sertoli cells. *Blood* **100**, 2617-2622.

Jiang, H., Zhang, X., Luo, J., Dong, C., Xue, J., Wei, W., Chen, J., Zhou, J., Gao, Y. and Yang, C. (2012). Knockdown of hMex-3A by small RNA interference suppresses cell proliferation and migration in human gastric cancer cells. *Mol. Med. Rep.* **6**, 575-580.

Jiao, Y., Bishop, C. E. and Lu, B. (2012a). Mex3c regulates insulin-like growth factor 1 (IGF1) expression and promotes postnatal growth. *Mol. Biol. Cell* **23**, 1404-1413.

Jiao, Y., George, S. K., Zhao, Q., Hulver, M. W., Hutson, S. M., Bishop, C. E. and Lu, B. (2012b). Mex3c mutation reduces adiposity and increases energy expenditure. *Mol. Cell. Biol.* **32**, 4350-4362.

Lablack, A., Bourdon, V., Defamie, N., Batias, C., Mesnil, M., Fenichel, P., Pointis, G. and Segretain, D. (1998). Ultrastructural and biochemical evidence for gap junction and connexin 43 expression in a clonal Sertoli cell line: a potential model in the study of junctional complex formation. *Cell Tissue Res.* **294**, 279-287.

Lécureuil, C., Fontaine, I., Crepieux, P. and Guillou, F. (2002). Sertoli and granulosa cell-specific Cre recombinase activity in transgenic mice. *Genesis* **33**, 114-118.

Lécuyer, E., Yoshida, H., Parthasarathy, N., Alm, C., Babak, T., Cerovina, T., Hughes, T. R., Tomancak, P. and Krause, H. M. (2007). Global analysis of mRNA localization reveals a prominent role in organizing cellular architecture and function. *Cell* **131**, 174-187.

Lee, N. P. Y. and Cheng, C. Y. (2004). Ectoplasmic specialization, a testis-specific cell-cell actin-based adherens junction type: is this a potential target for male contraceptive development? *Hum. Reprod. Update* **10**, 349-369.

Li, M. W. M., Mruk, D. D., Lee, W. M. and Cheng, C. Y. (2010). Connexin 43 is critical to maintain the homeostasis of the blood-testis barrier via its effects on tight junction reassembly. *Proc. Natl. Acad. Sci. U.S.A.* **107**, 17998-18003.

Meng, J., Holdcraft, R. W., Shima, J. E., Griswold, M. D. and Braun, R. E. (2005). Androgens regulate the permeability of the blood-testis barrier. *Proc. Natl. Acad. Sci. U.S.A.* **102**, 16696-16700.

Mather, J. P. (1980). Establishment and characterization of two distinct mouse testicular epithelial cell lines. *Biol. Reprod.* **23**, 243-252.

Mochizuki, N., Yamashita, S., Kurokawa, K., Ohba, Y., Nagai, T., Miyawaki, A. and Matsuda, M. (2001). Spatio-temporal images of growth-factor-induced activation of Ras and Rap1. *Nature* **411**, 1065-1068.

Nakagawa, A., Nagaosa, K., Hirose, T., Tsuda, K., Hasegawa, K., Shiratsuchi, A. and Nakanishi, Y. (2004). Expression and function of class B scavenger receptor type I on both apical and basolateral sides of the plasma membrane of polarized testicular Sertoli cells of the rat. *Dev. Growth Differ.* **46**, 283-298.

Nakanishi, Y. and Shiratsuchi, A. (2004). Phagocytic removal of apoptotic spermatogenic cells by Sertoli cells: mechanisms and consequences. *Biol. Pharm. Bull.* **27**, 13-16.

Newton, S. C., Blaschuk, O. W. and Millette, C. F. (1993). N-cadherin mediates Sertoli cell-spermatogenic cell adhesion. *Dev. Dyn.* **197**, 1-13.

Nony, P., Gaude, H., Rossel, M., Fournier, L., Rouault, J. P. and Billaud, M. (2003). Stability of the Peutz-Jeghers syndrome kinase LKB1 requires its binding to the molecular chaperones Hsp90/Cdc37. *Oncogene* **22**, 9165-9175.

O'Connor, A. E. and de Kretser, D. M. (2004). Inhibins in normal male physiology. *Semin. Reprod. Med.* **22**, 177-185.

Ohba, Y., Kurokawa, K. and Matsuda, M. (2003). Mechanism of the spatio-temporal regulation of Ras and Rap1. *EMBO J.* **22**, 859-869.

Pagano, J. M., Farley, B. M., Essien, K. I. and Ryder, S. P. (2009). RNA recognition by the embryonic cell fate determinant and germline totipotency factor MEX-3. *Proc. Natl. Acad. Sci. U.S.A.* **106**, 20252-20257.

Park, H.-O. and Bi, E. (2007). Central roles of small GTPases in the development of cell polarity in yeast and beyond. *Microbiol. Mol. Biol. Rev.* **71**, 48-96.

Park, D., Tosello-Trampont, A. C., Elliott, M. R., Lu, M., Haney, L. B., Ma, Z., Klibanov, A. L., Mandell, J. W. and Ravichandran, K. S. (2007). BAI1 is an engulfment receptor for apoptotic cells upstream of the ELMO/Dock180/Rac module. *Nature* **450**, 430-434.

Patek, C. E., Kerr, J. B., Gosden, R. G., Jones, K. W., Hardy, K., Muggleton-Harris, A. L., Handyside, A. H., Whittingham, D. G. and Hooper, M. L. (1991). Sex chimaerism, fertility and sex determination in the mouse. *Development* **113**, 311-325.

Pereira, B., Le Borgne, M., Chartier, N. T., Billaud, M. and Almeida, R. (2013a). MEX-3 proteins: recent insights on novel post-transcriptional regulators. *Trends Biochem. Sci.* **38**, 477-479.

Pereira, B., Sousa, S., Barros, R., Carreto, L., Oliveira, P., Oliveira, C., Chartier, N. T., Plateroti, M., Rouault, J.-P., Freund, J.-N. et al. (2013b). CDX2 regulation by the RNA-binding protein MEX3A: impact on intestinal differentiation and stemness. *Nucleic Acids Res.* **41**, 3986-3999.

Plotton, I., Sanchez, P., Perrard, M. H., Durand, P. and Lejeune, H. (2005). Quantification of stem cell factor mRNA levels in the rat testis: usefulness of clusterin mRNA as a marker of the amount of mRNA of Sertoli cell origin in post pubertal rats. *J. Endocrinol.* **186**, 131-143.

Polakis, P. G., Rubinfeld, B., Evans, T. and McCormick, F. (1991). Purification of a plasma membrane-associated GTPase-activating protein specific for rap1/Krev-1 from HL60 cells. *Proc. Natl. Acad. Sci. U.S.A.* **88**, 239-243.

Ray, D., Kazan, H., Cook, K. B., Weirauch, M. T., Najafabadi, H. S., Li, X., Gueroussov, S., Albu, M., Zheng, H., Yang, A. et al. (2013). A compendium of RNA-binding motifs for decoding gene regulation. *Nature* **499**, 172-177.

Rubinfeld, B., Munemitsu, S., Clark, R., Conroy, L., Watt, K., Crosier, W. J., McCormick, F. and Polakis, P. (1991). Molecular cloning of a GTPase activating protein specific for the Krev-1 protein p21rap1. *Cell* **65**, 1033-1042.

Russell, L. D. and Peterson, R. N. (1985). Sertoli cell junctions: morphological and functional correlates. *Int. Rev. Cytol.* **94**, 177-211.

Steininger, T. S., Stutz, H. and Kerschbaum, H. H. (2011). Beta-adrenergic stimulation suppresses phagocytosis via Epac activation in murine microglial cells. *Brain Res.* **1407**, 1-12.

Stelzl, U., Worm, U., Lalowski, M., Haenig, C., Brembeck, F. H., Goehler, H., Stroedicke, M., Zenkner, M., Schoenherr, A., Koeppen, S. et al. (2005). A human protein-protein interaction network: a resource for annotating the proteome. *Cell* **122**, 957-968.

van Triest, M., de Rooij, J. and Bos, J. L. (2001). Measurement of GTP-bound Ras-like GTPases by activation-specific probes. *Methods Enzym.* **333**, 343-348.

Wang, H., Singh, S. R., Zheng, Z., Oh, S.-W., Chen, X., Edwards, K. and Hou, S. X. (2006). Rap-GEF signaling controls stem cell anchoring to their niche through regulating DE-cadherin-mediated cell adhesion in the Drosophila testis. *Dev. Cell* **10**, 117-126.

Weiss, M., Vigier, M., Hue, D., Perrard-Sapori, M. H., Marret, C., Avallet, O. and Durand, P. (1997). Pre- and postmeiotic expression of male germ cell-specific genes throughout 2-week cocultures of rat germinal and Sertoli cells. *Biol. Reprod.* **57**, 68-76.

Yefimova, M. G., Sow, A., Fontaine, I., Guilleminot, V., Martinat, N., Crepieux, P., Canepa, S., Maurel, M.-C., Fouchécourt, S., Reiter, E. et al. (2008). Dimeric transferrin inhibits phagocytosis of residual bodies by testicular rat Sertoli cells. *Biol. Reprod.* **78**, 697-704.

Yoon, J. H., Abdelmohsen, K., Kim, J., Yang, X., Martindale, J. L., Tominaga-Yamanaka, K., White, E. J., Orjalo, A. V., Rinn, J. L., Kreft, S. G. et al. (2013). Scaffold function of long non-coding RNA HOTAIR in protein ubiquitination. *Nat Commun.* **4**, 2939.

Supplemental information

Supplemental material and methods

Mice Generation and Genotyping.

For generation of Mex-3b null mice, the second exon was flanked by *loxP* sequences, and the Neo selectable marker was removed by transient expression of Cre recombinase in the ES cells. The *Mex-3b* null allele was obtained by breeding conditional floxed *Mex-3b* animals with Nestin-Cre mice expressing Cre in the germ line (Betz et al., 1996). Heterozygous *Mex-3b +/-* animals negative for Cre were bred to each other to obtain the *Mex-3b* knock-out mice. For the generation of Sertoli cells specific *Mex-3b* null mice, conditional *Mex-3b* floxed mice were bred with AMH-Cre mice expressing Cre (Lecureuil et al., 2002).

Embryos and mice were genotyped by multiplex PCR using 3 primers as described in figure 1A:

Mex-3b (1) 5' (GCTCAGTTGGATACCAGCAGC)

Mex-3b (2) 3' (CAAGCATCGTCAGCTGTGTGTAATG)

Mex-3b (3) 5' (GGGCCTTTAACCTCATGGTC)

The wild-type allele produced a band of 433 bp, the floxed allele a band of 559 bp and the knock-out allele a band of 387 bp. Survival of wild type, *Mex-3b +/-* and *Mex-3b -/-* mice was monitored for 60 days after birth.

Transfection and Infection.

For transfection, cells were plated for 24h and plasmids transfected into cells using ExGen 500 (Upstate Biotechnologies) or Jet Pei (Ozyme) according to the manufacturer's instructions. For infections, cells were plated for 24h and lentiviruses were added to the culture media at a MOI of 30 in the presence of polybren (8 µg/ml). Expression of GFP proteins was controlled by microscopy and Western blot.

Histological sections and Staining.

Serial sections (3µm) were stained with Periodic Acid-Schiff and Gill's Hematoxilin solution (Sigma-Aldrich). For immunohistochemistry, sections were deparafinized, deshydrated and incubated with primary antibody (mouse anti-vimentin (1:100,

Sigma-Aldrich)). The ABC MOM and AEC peroxidase substrate kits (Vector laboratories) and Hematoxylin QS were used.

Biotin Tracer Studies.

Mice (5 months old) were anesthetized and their testes exposed. Before injection of 50 µl of 10 mg/ml EZ-Link Sulfo-NHS-LC-Biotin (Pierce Chemical Co.), into the interstitium of one testis and 50 µl of 1 mM $CaCl_2$ in PBS in the other, as a control. After 30 min the animals were euthanized, and their testes were immediately removed and frozen on dry ice. Cryosections of 5-µm thickness were fixed for 10 min with 4% PFA, rinced with PBS and treated with Alexa Fluor 488 streptavidin. The sections were rinsed twice with PBS for 10 min and mounted in DAPI containing mounting medium.

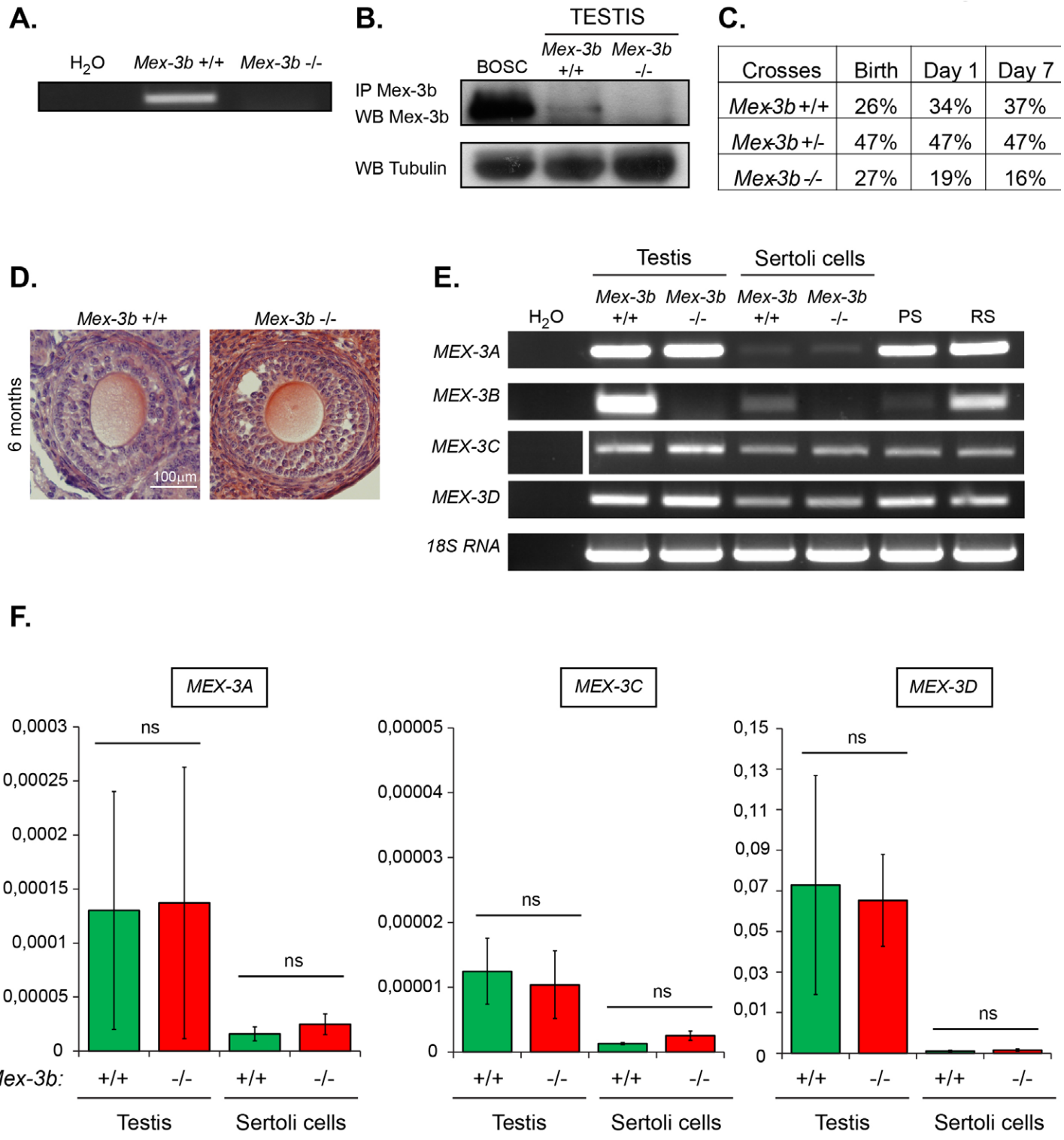

Figure S1. Mex-3b depletion affects viability and fertility in both male and female mice.

(A) RT-qPCR analysis of *Mex-3b* transcripts isolated from MEFs cells. (B) Western blot analysis of endogenous MEX-3B (indicated by black arrow) immunoprecipitated from BOSC cells and from whole mouse testis with the indicated *Mex-3b* genotypes. One representative experiment of three is shown. (C) Table of breeding and survival data of *Mex-3b* deficient mice. The average genotypes of offspring from *Mex-3b +/-* mating at birth to day 7. (D) Hematoxilin and Scarlett Eosin staining of secondary follicle cross section from 6 months-old mice with the indicated *Mex-3b* genotypes.. (E) RT-PCR analysis of the levels of the four distinct *Mex-3* mRNA in the testis of wt and *Mex-3b* deficient mice, purified Sertoli cells and purified pachytene spermatocytes (PS) and round spermatids (RS). (F) RT-qPCR analysis of *Mex-3a, c and d* transcripts isolated from testis and purified Sertoli cells of indicated *Mex-3b* genotypes 3 months-old mice.

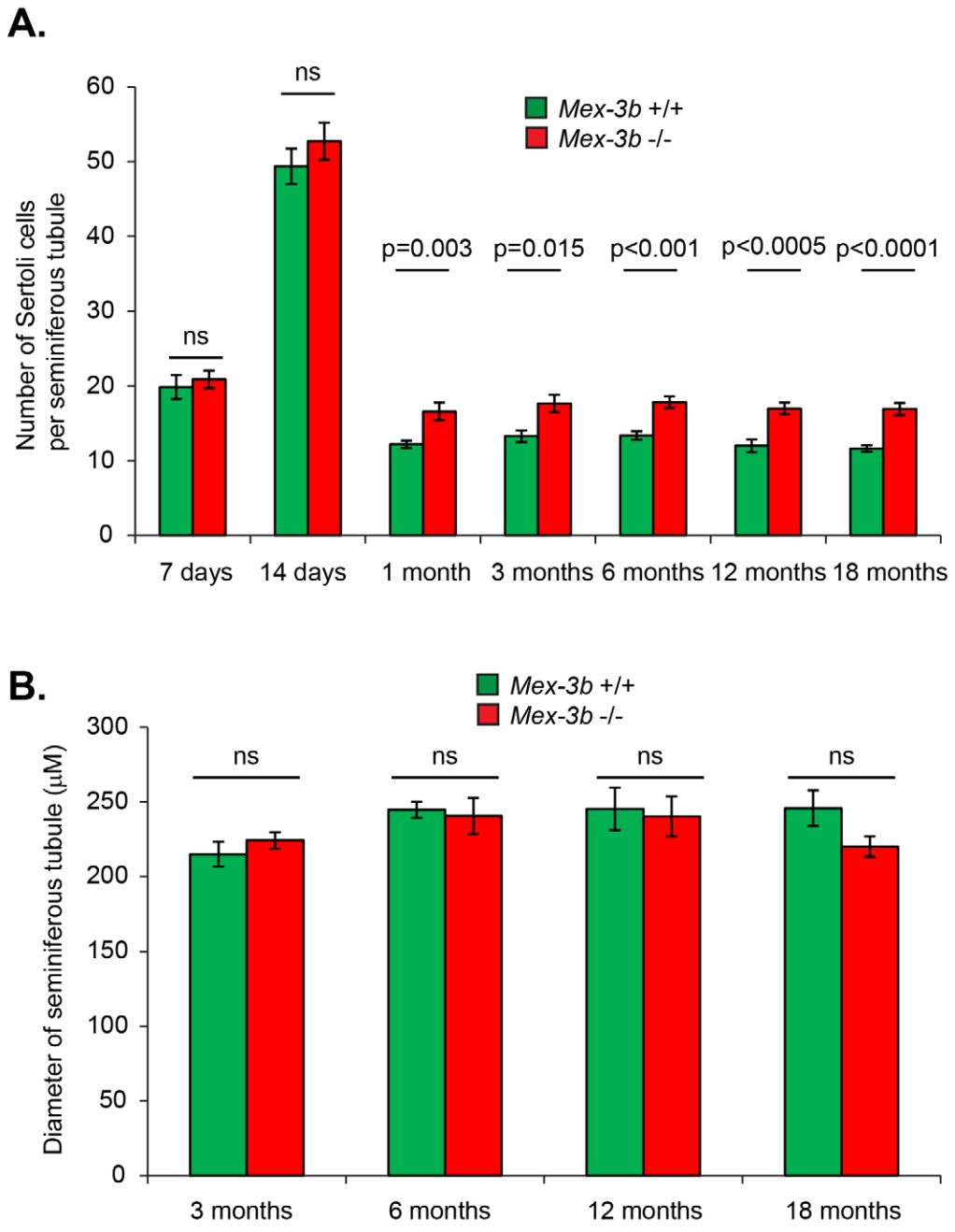

Figure S2. *Mex-3b* deficient seminiferous tubules have more Sertoli cells but an identical diameter compare to control.

(A) Counting of Sertoli cells per seminiferous tubules of wt and *Mex-3b* deficient mice at different ages (d for days and m for months). Sertoli cells were identified as cells positively stained for vimentin (n= 6 mice/group, 30 seminiferous tubules/ mouse). (B) Representation of the mean seminiferous tubules diameter of wt and *Mex-3b* deficient mice at different ages (d for days and m for months) (n= 6 mice/group, 30 seminiferous tubules/mouse).

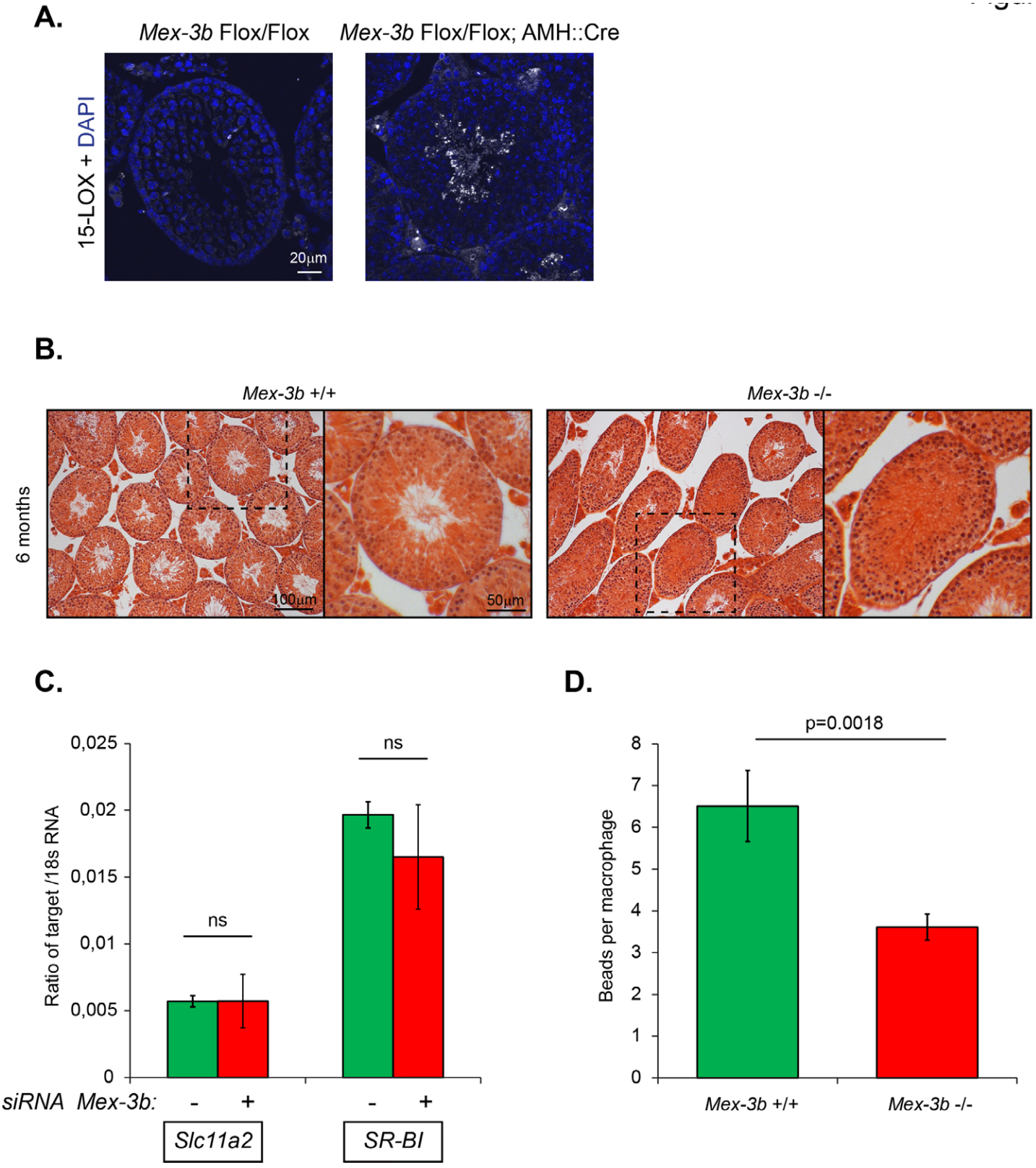

Figure S3. Deletion of *Mex-3b* affects phagocytosis in Sertoli cells.

(A) Immunodetection of 15-Lipoxygenase (15-LOX) on cross-sections of mouse testes with the indicated *Mex-3b* genotypes at 6 months old. (B) Hematoxilin and Scarlett Eosin staining of testis cross section from mice with the indicated *Mex-3b* genotypes. (C) RT-qPCR analysis of *Slc11a* and *SR-BI* transcripts isolated from murine TM4 cells depleted in *Mex-3b* by siRNA. All levels were normalized to the level of *18S* mRNA. One representative experiment of three is shown. Scale bars and P values with s.e.m are indicated. (D). Phagocytosis assay on wild type and *Mex-3b -/-* isolated macrophages Histogram indicates the average numbers of engulfed fluorescent beads per phalloidin-TRITC stained cell (n=100 cells per condition).

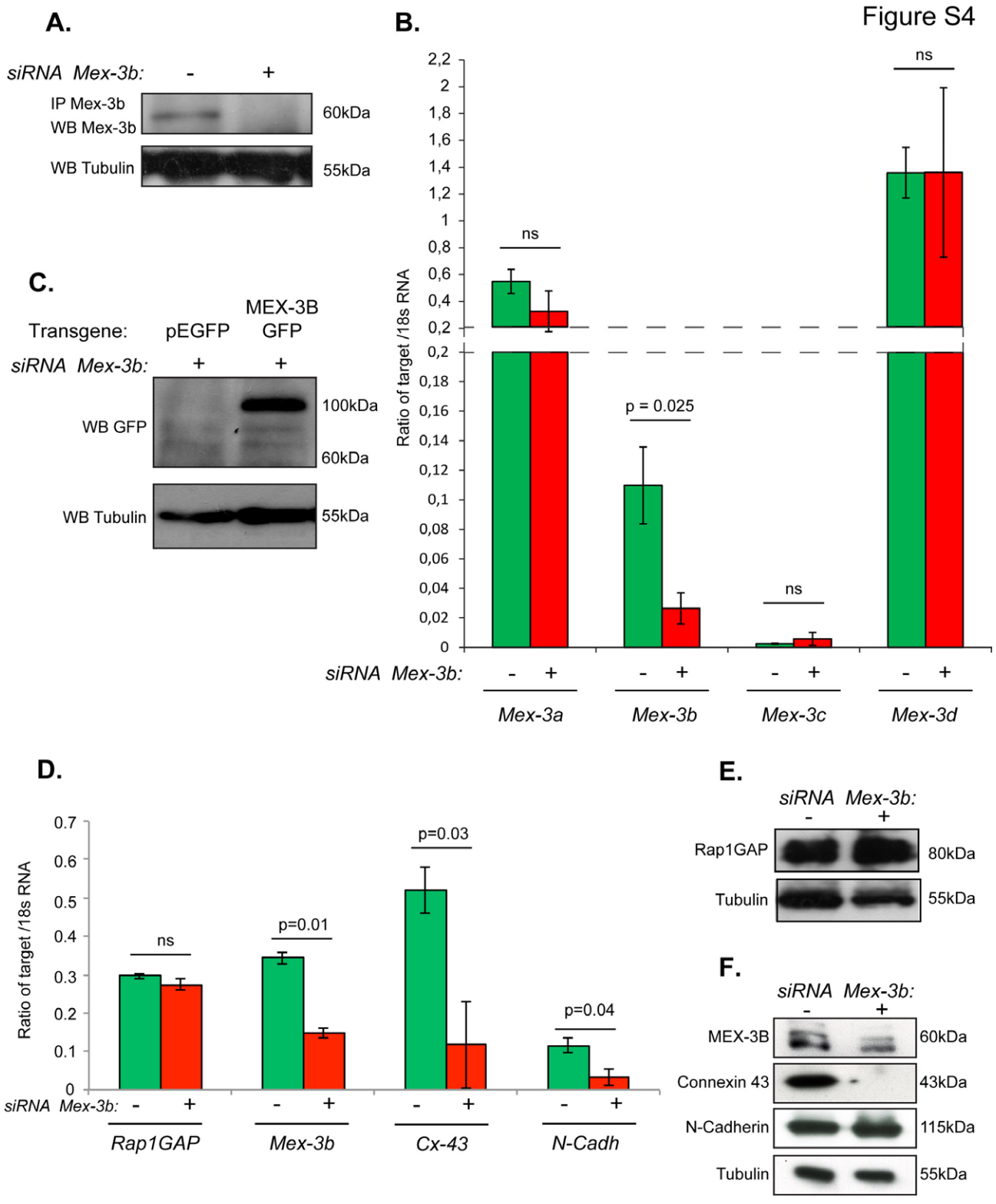

Figure S4. Specific inhibition of mouse *Mex-3b* expression and rescue with human MEX-3B in TM4 cells.

(A) Mex-3b protein level was determined by immunoprecipitation and Western blot analysis in TM4 cells 48h after siRNA treatment. (B) RT-qPCR analysis of *Mex-3a, b, c* and *d* transcripts isolated from murine TM4 cells depleted in *Mex-3b* by siRNA. All levels were normalized to the level of *18S* mRNA. One representative experiment of three is shown. (C) Expression of human MEX-3B-GFP construct in TM4 cells knocked down for mouse *Mex-3b* expression after lentiviruses infection (n=3 experiments). Tubulin was used as a loading control. (D) RT-qPCR analysis of *Rap1GAP, Mex-3b, Connexin-43 and N-Cadherin* transcripts isolated from murine TM4 cells depleted in *Mex-3b* by siRNA (n=3 experiments). All levels were normalized to the level of *18S* mRNA. (E) Western blot analysis of Rap1GAP protein in TM4 cells depleted in *Mex-3b*. Tubulin was used as a loading control. (F) Western blot analysis of MEX-3B, Connexin-43 and N-Cadherin proteins in TM4 cells depleted in *Mex-3b*. Tubulin was used as a loading control.

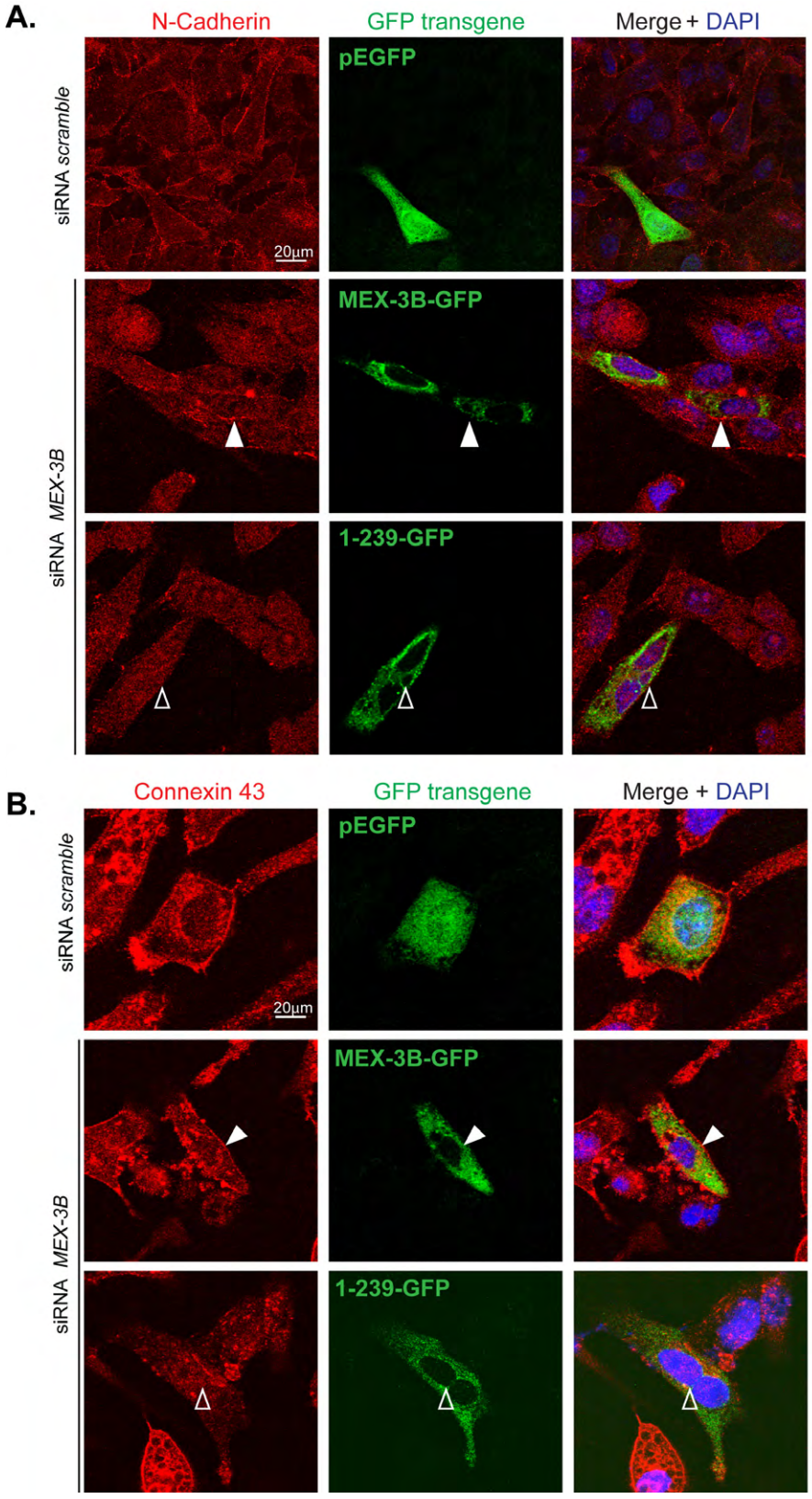

Figure S5. Mex-3b binding to RAP1GAP is required for junctions protein localization.

Confocal microscope images of TM4 cells inhibited for endogenous *Mex-3b* by siRNA and re-expressing the human MEX-3B protein full length or truncated (1-239) fused to GFP. N-cadherin (A) and Connexin 43 (B) were immunostained and counterstained with DAPI. Upon Mex-3b depletion by *si RNA,* the re-expression of the full-length construct allows the relocalization of junction proteins to the membrane (white arrowheads), wheras the re-expression of the 1-239 mutant does not (empty arrowheads).

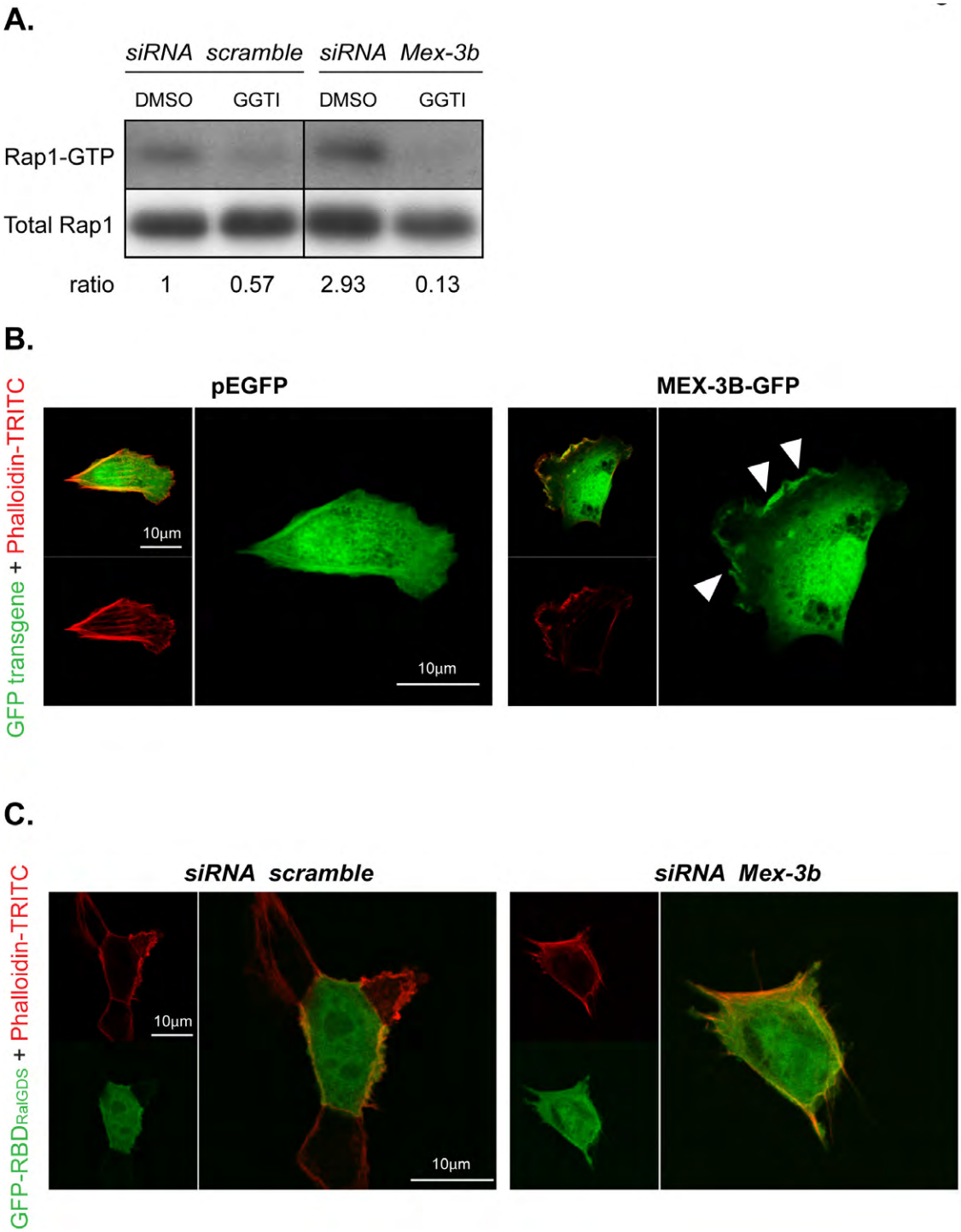

Figure S6. Mex-3b regulates Rap1 activity.

(A) Rap1-GTP pull down from lysates of TM4 cells transfected with either *scramble* or *Mex-3b* siRNA before treatment with the Rap1 inhibitor, GGTI-298. The ratio of Rap1-GTP / Total Rap1 for each condition is indicated. (B) After a short serum stimulation, TM4 cells expressing the indicated GFP constructs were fixed and stained with phalloidin-TRITC prior observation by confocal microscopy. White arrowheads indicate the plasma membrane localization of MEX-3B-GFP.

(C) Localization of GFP-RBD_{ralGDS} in TM4 cells knocked down for *Mex-3b* expression by siRNA after GGTI-298 treatment. Cells were exposed to phalloidin-TRITC prior observation by confocal microscopy.

Betz, U. A., Vosshenrich, C. A., Rajewsky, K. and Müller, W. (1996). Bypass of lethality with mosaic mice generated by Cre-loxP-mediated recombination. *Curr. Biol.* **6**, 1307–16.

Lecureuil, C., Fontaine, I., Crepieux, P. and Guillou, F. (2002). Sertoli and granulosa cell-specific Cre recombinase activity in transgenic mice. *Genesis* **33**, 114–118.

Table S1. RT-PCR primer sequences

	LEFT	RIGHT
Mex-3a	TTGATCAACTCTGCCTCCTG	TCCCAGTCACCATGAACACT
Mex-3b	GAGACTCTGGATGACCAAAGA	CGTTGAGAGCCGTGTTCTTG
Mex-3c	CTGTACGGCGGGGACGATG	ACCAGGCAGATTAGGACTACA
Mex-3d	AGTTGAACGTGATCGGGAGT	CCATCTCCACATCCTCCTTG
Clusterin	AACAGCTTCACCACCACCTC	CGAAGATGCTCAACACCTCA
Transferrin	GGCATCGGACACTAGCATCA	TGCCATCAGGGCAGAGCAAC
Inhibin	TCAGCCCAGCTGTGGTTCCACA	AGCCCAGCTCTTGGAAGGAGAT
LDHA	TTCCACTGCTCCTTGTCTGC	ACAGTCCACACTGCAAGCTG
Vimentin	AAGGAAGAGATGGCTCGTCA	TTGAGTGGGTGTCAACCAGA
18S	CGACGACCCATTCGAACGTCT	GCTATTGGAGCATGGAATTACCG
Rap1GAP	GAAAAGATGCAGGGAAGCAG	GTTGGTGCCTTCAATCCAGT
Slc11a2	TCCCCATTCCTGAGGAGGAG	ATCCGTGGGACCTTGGGATA
SR-BI	TCTTCACTGTCTTCACGGGC	CATGAAGGGTGCCCACATCT
Connexin-43	CTATCTTTGAGGTGGCCTTC	TCGCTCTTTCCCTTAACCCG
N-Cadherin	CGGACTCCGAGGCCCGCTAT	GCCTCCACAGACGCCTGAAGC